

h-Edit: Effective and Flexible Diffusion-Based Editing via Doob’s *h*-Transform

Toan Nguyen* Kien Do* Duc Kieu Thin Nguyen

{k.nguyen, k.do, v.kieu, thin.nguyen}@deakin.edu.au

Applied Artificial Intelligence Institute (A2I2), Deakin University, Australia

* Equal contribution

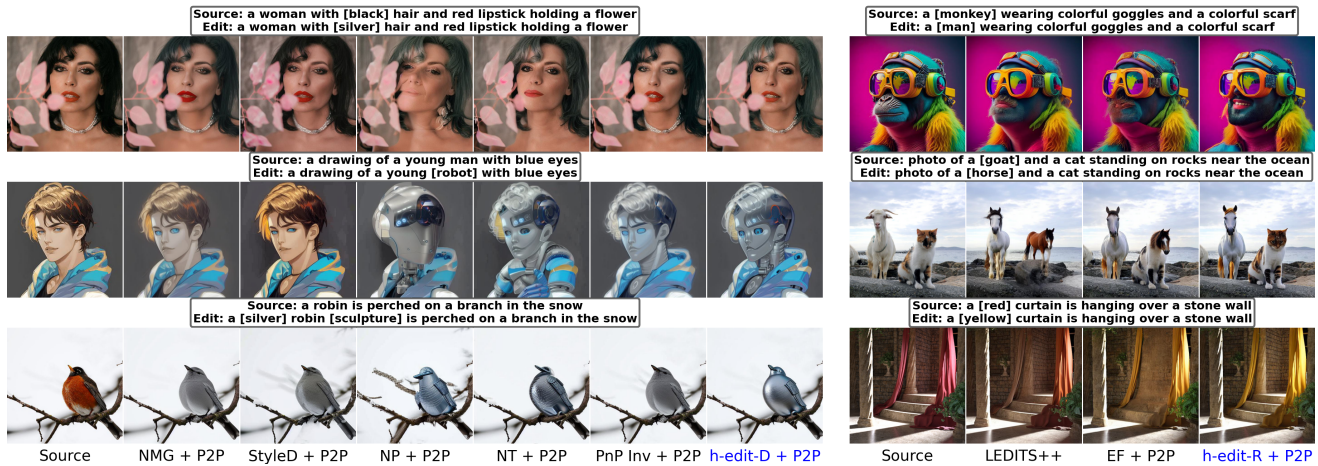


Figure 1. Qualitative comparison between *h*-Edit and other training-free editing baselines. Our method achieves more accurate and faithful edits than the baselines. Additional visualizations are provided in the Appendix.

Abstract

We introduce a theoretical framework for diffusion-based image editing by formulating it as a reverse-time bridge modeling problem. This approach modifies the backward process of a pretrained diffusion model to construct a bridge that converges to an implicit distribution associated with the editing target at time 0. Building on this framework, we propose *h*-Edit, a novel editing method that utilizes Doob’s *h*-transform and Langevin Monte Carlo to decompose the update of an intermediate edited sample into two components: a “reconstruction” term and an “editing” term. This decomposition provides flexibility, allowing the reconstruction term to be computed via existing inversion techniques and enabling the combination of multiple editing terms to handle complex editing tasks. To our knowledge, *h*-Edit is the first training-free method capable of performing simultaneous text-guided and reward-model-based editing. Extensive experiments, both quantitative and qualitative, show that *h*-Edit outperforms state-of-the-art baselines in terms of editing effectiveness and faithfulness. Our source code is available at <https://github.com/nktoan/>

h-edit.

1. Introduction

Diffusion models [22, 62, 65] have established themselves as a powerful class of generative models, achieving state-of-the-art performance in image generation [64]. When combined with classifier-based [12] or classifier-free guidance [21], these models offer enhanced control, enabling a wide range of applications including conditional generation [79, 80], image-to-image translation [8, 56], and image editing [19, 23, 44]. A prominent example is large-scale text-guided diffusion models [47, 57] like Stable Diffusion (SD) [55], which have gained widespread popularity for their ability to produce diverse high-quality images that closely align with specified natural language descriptions.

However, leveraging pretrained text-guided diffusion models for image editing presents significant challenges, particularly in balancing effective editing with faithful preservation of the unrelated content in the original image. Moreover, combining text-guided editing with other forms

of editing to handle more complex requirements remains a difficult task. Although recent advances in training-free image editing have been proposed [7, 19, 24, 27, 46, 70], most of these efforts focus on improving reconstruction quality through better inversion techniques or attention map adjustment, while leaving the editing part largely unchanged. Additionally, many of these methods are based on heuristics or intuition, lacking a clear theoretical foundation to justify their effectiveness. This limitation restricts the generalization of these approaches to more complex scenarios where multiple types of editing must be applied.

In this work, we aim to fill the theoretical gap by introducing a theoretical framework for image editing, formulated as a *reverse-time bridge modeling* problem. Our approach modifies the *backward* process of a pretrained diffusion model using Doob’s *h*-transform [15, 54, 58] to create a bridge that converges to the distribution $p(x_0)h(x_0, 0)$ at time 0. Here, $p(x_0)$ represents the realism of x_0 , while $h(x_0, 0)$ captures the probability that x_0 has the target property. To perform editing, we first map the original image x_0^{orig} to its prior x_T^{orig} through the diffusion forward process. Starting from $x_T^{\text{edit}} = x_T^{\text{orig}}$, we follow the bridge to generate an edited image x_0^{edit} by sampling from its transition kernel $p^h(x_{t-1}|x_t)$ using Langevin Monte Carlo (LMC) [53, 74].

Building on the decomposability of $p^h(x_{t-1}|x_t)$, we propose *h-Edit* - a novel editing method that disentangles the update of x_{t-1}^{edit} into a “*reconstruction*” term x_{t-1}^{base} (capturing editing faithfulness) and an “*editing*” term (capturing editing effectiveness). This design provides significant flexibility, as the editing term can be easily customized for different tasks with minimal interference in non-edited regions. *h-Edit* updates can be either explicit or implicit, with $\nabla \log h(x_t, t)$ and $\nabla \log h(x_{t-1}, t-1)$ being the corresponding editing terms, respectively. In the latter case, *h-Edit* can also be interpreted from an optimization perspective where $\log h(x_{t-1}, t-1)$ is maximized w.r.t. x_{t-1} , taking x_{t-1}^{base} as the initial value. This allows for multiple optimization steps to enhance editing effectiveness.

While x_{t-1}^{base} can generally be estimated by leveraging existing inversion techniques [24, 27, 46, 64], the computation of $\nabla \log h(x_{t-1}, t-1)$ depends on the chosen *h*-function. In this work, we present several key designs of the *h*-function tailored to popular editing tasks, including text-guided editing with SD and editing with external reward models on clean data. Furthermore, by treating $\log h$ as a negative energy function, we can easily combine multiple *h*-functions to create a “product of *h*-experts”, which enables compositional editing.

Through extensive experiments on a range of editing tasks - including text-guided editing, combined text-guided and style editing, and face swapping - we demonstrate strong editing capabilities of *h-Edit*. Both quantitative and qualitative results indicate that *h-Edit* not only significantly

outperforms existing state-of-the-art methods in text-guided editing but also excels in the two other tasks. Our method effectively handles various difficult editing cases in the PIE-Bench dataset where existing methods fall short. To our knowledge, *h-Edit* is the *first* diffusion-based training-free editing method that supports simultaneous text-guided and reward-model-based editing.

2. Preliminaries

2.1. Diffusion Models

Diffusion models [22, 62, 65] iteratively transform the data distribution $p(x_0)$ into the prior distribution $p(x_T) = \mathcal{N}(0, \mathbf{I})$ via a *predefined forward* stochastic process characterized by $p(x_t|x_{t-1})$, and learn the *reverse* transition distribution $p_\theta(x_{t-1}|x_t)$ to map $p(x_T)$ back to $p(x_0)$. Given the Gaussian form and Markov property of $p(x_t|x_{t-1})$, $p(x_t|x_0)$ is a Gaussian distribution $\mathcal{N}(a_t x_0, \sigma_t^2 \mathbf{I})$, allowing x_t to be sampled from $p(x_t|x_0)$ as follows:

$$x_t = a_t x_0 + \sigma_t \epsilon \quad (1)$$

with $\epsilon \sim \mathcal{N}(0, \mathbf{I})$. In DDPM [22], $a_t = \sqrt{\bar{\alpha}_t}$ and $\sigma_t = \sqrt{1 - \bar{\alpha}_t}$. $p_\theta(x_{t-1}|x_t)$ is parameterized as a Gaussian distribution $\mathcal{N}(\mu_{\theta, \omega, t, t-1}(x_t), \omega_{t, t-1}^2 \mathbf{I})$ with the mean

$$\mu_{\theta, \omega, t, t-1}(x_t) := \frac{a_{t-1}}{a_t} x_t + \left(\sqrt{\sigma_{t-1}^2 - \omega_{t, t-1}^2} - \frac{\sigma_t a_{t-1}}{a_t} \right) \epsilon_\theta(x_t, t) \quad (2)$$

Here, $\omega_{t, t-1} = \lambda \sigma_{t-1} \sqrt{1 - \frac{a_t^2 \sigma_{t-1}^2}{a_{t-1}^2 \sigma_t^2}}$ with $\lambda \in [0, 1]$. $\lambda = 0$ and $\lambda = 1$ correspond to DDIM sampling [64] and DDPM sampling [22], respectively. Eq. 2 implies that $x_{t-1} \sim p_\theta(x_{t-1}|x_t)$ is given by:

$$x_{t-1} = \mu_{\theta, \omega, t, t-1}(x_t) + \omega_{t, t-1} z_t \quad (3)$$

with $z_t \sim \mathcal{N}(0, \mathbf{I})$. Diffusion models support conditional generation via classifier-based [12] and classifier-free [21] guidances. The latter is more prevalent, with Stable Diffusion (SD) [55] serving as a notable example. In SD, both the unconditional and text-conditional noise networks - $\epsilon_\theta(x_t, t, \emptyset)$ and $\epsilon_\theta(x_t, t, c)$ - are learned, and their linear combination $\tilde{\epsilon}_\theta(x_t, t, c) := w \epsilon_\theta(x_t, t, c) + (1 - w) \epsilon_\theta(x_t, t, \emptyset)$, with $w > 0$ denoting the guidance weight, is often used for sampling. This results in the following sampling step for SD:

$$x_{t-1} = \tilde{\mu}_{\theta, \omega, t, t-1}(x_t, c) + \omega_{t, t-1} z_t \quad (4)$$

where $\tilde{\mu}_{\theta, \omega, t, t-1}$ follows the same form as $\mu_{\theta, \omega, t, t-1}(x_t)$ in Eq. 2 but with $\epsilon_\theta(x_t, t)$ replaced by $\tilde{\epsilon}_\theta(x_t, t, c)$.

2.2. Image Editing with Stable Diffusion

The design of SD facilitates text-guided image editing which involves modifying some attributes of the original image x_0^{orig} while preserving other features (e.g., background) by adjusting the corresponding text prompt c^{orig} . A naive approach is mapping x_0^{orig} to x_T^{orig} using DDIM inversion w.r.t. c^{orig} , followed by generating x_0^{edit} from $x_T^{\text{edit}} = x_T^{\text{orig}}$ via DDIM sampling (Eq. 4) w.r.t. c^{edit} - the edited version of c^{orig} . DDIM inversion is the reverse of DDIM sampling, which achieves nearly exact reconstruction in the unconditional case [19, 64]. For SD, DDIM inversion is expressed as:

$$x_t = \frac{a_t}{a_{t-1}}x_{t-1} + \left(\sigma_t - \frac{\sigma_{t-1}a_t}{a_{t-1}} \right) \tilde{\epsilon}_\theta(x_{t-1}, t-1, c) \quad (5)$$

However, there is a mismatch between $\tilde{\epsilon}_\theta(x_t, t, c^{\text{edit}})$ and $\tilde{\epsilon}_\theta(x_{t-1}, t-1, c^{\text{orig}})$ during sampling and inversion, causing x_0^{edit} to be significantly different from x_0^{orig} . Therefore, much of the research on SD text-guided image editing focuses on improving reconstruction. These inversion methods can be broadly classified into deterministic-inversion-based [14, 27, 38, 46] and random-inversion-based [24, 75] techniques. Edit Friendly (EF) [24] - a state-of-the-art random-inversion-based method - can be formulated under the following framework:

$$u_t^{\text{orig}} = x_{t-1}^{\text{orig}} - \tilde{\mu}_{\theta, \omega, t, t-1}(x_t^{\text{orig}}, c^{\text{orig}}) \quad (6)$$

$$x_{t-1}^{\text{edit}} = \tilde{\mu}_{\theta, \omega, t, t-1}(x_t^{\text{edit}}, c^{\text{edit}}) + u_t^{\text{orig}} \quad (7)$$

Here, u_t^{orig} serves as a residual term that ensures non-edited features from x_{t-1}^{orig} are retained in the edited version x_{t-1}^{edit} . For EF, the set $\left\{ x_t^{\text{orig}} \right\}_{t=1}^T$ is constructed by sampling x_t^{orig} from $p(x_t|x_0^{\text{orig}})$ for each t in parallel. Interestingly, this set can also be built sequentially through DDIM inversion as per Eq. 5 (with c^{orig} replacing c).

2.3. Diffusion Bridges and Doob's h -transform

Although various definitions of bridges exist in the literature [10, 32, 36, 39, 42, 67], we adopt the perspective of [32, 41, 85] and regard bridges as special stochastic processes that converge to a *predefined* sample \hat{x}_T at time T almost surely. A bridge can be derived from a *base* (or *reference*) Markov process through Doob's h -transform [15, 54, 58]. If the base process is a diffusion process described by the SDE $dx_t = f(x_t, t)dt + g(t)dw_t$, the corresponding bridge is governed by the following SDE:

$$dx_t = \left(f(x_t, t) + g(t)^2 \nabla \log h(x_t, t) \right) dt + g(t) dw_t \quad (8)$$

where $h(x_t, t) = p(\hat{x}_T|x_t)$. When $f(x_t, t)$ is a linear function of x_t , $h(x_t, t)$ simplifies into a Gaussian distribution that can be expressed in closed form [85].

3. Method

3.1. Editing as Reverse-time Bridge Modeling

In this section, we introduce a *novel* theoretical framework for image editing with diffusion models by framing it as a *reverse-time bridge modeling* problem. This idea stems from our insight that we can generate images x_0 exhibiting the target properties \mathcal{Y} (e.g., style, shape, color, object type, ...) by constructing a bridge from the *backward* process that converges to an *implicit* distribution associated with \mathcal{Y} . Our framework stands apart from most existing bridge models [41, 63, 85] which focus solely on the (non-parameterized) *forward* process and assume an *explicit* target sample \hat{x}_0 (or set of samples $\{\hat{x}_0\}$).

To construct this bridge, we modify the transition distribution $p_\theta(x_{t-1}|x_t)$ of the backward process using Doob's h -transform [15, 58] as follows:

$$p_\theta^h(x_{t-1}|x_t) = p_\theta(x_{t-1}|x_t) \frac{h(x_{t-1}, t-1)}{h(x_t, t)} \quad (9)$$

Here, $h(x_t, t)$ is a positive real-valued function that satisfies the following conditions for all $t \in [1, T]$:

$$h(x_t, t) = \int p_\theta(x_{t-1}|x_t) h(x_{t-1}, t-1) dx_{t-1} \quad (10)$$

$$h(x_0, 0) = p_Y(x_0) \quad (11)$$

where $p_Y(x_0)$ is a *predefined* distribution quantifying how likely x_0 possesses the attributes \mathcal{Y} . $p_Y(x_0) = 0$ if x_0 does not have the attributes \mathcal{Y} and > 0 otherwise. For clarity in the subsequent discussion, we will omit the parameter θ in $p_\theta(x_{t-1}|x_t)$ and $p_\theta^h(x_{t-1}|x_t)$, referring to them simply as $p(x_{t-1}|x_t)$ and $p^h(x_{t-1}|x_t)$.

It can be shown that $h(x_t, t) = \mathbb{E}_{p(x_0|x_t)}[h(x_0, 0)]$ (Appdx. A.1) and the bridge constructed in this manner forms a reverse-time Markov process with the transition distribution $p^h(x_{t-1}|x_t)$. At time 0, this process converges to a distribution formally stated in Proposition 1 below:

Proposition 1. *Consider a reverse-time Markov process with the transition distribution $p(x_{t-1}|x_t)$ and a positive real-value function $h(x_t, t)$ satisfying Eqs. 10, 11 for all $t \in [1, T]$. If we construct a bridge from this Markov process such that its transition distribution $p^h(x_{t-1}|x_t)$ is defined as in Eq. 9, then the bridge is also a reverse-time Markov process. Moreover, if the distribution at time T of the bridge, $p^h(x_T)$, is set to $\frac{p(x_T)h(x_T, T)}{\mathbb{E}_{p(x_0)}[h(x_0, 0)]}$, then $p^h(x_t) = \frac{p(x_t)h(x_t, t)}{\mathbb{E}_{p(x_0)}[h(x_0, 0)]}$ for all $t \in [0, T]$.*

Proof. The detailed proof is provided in Appdx. A.2. \square

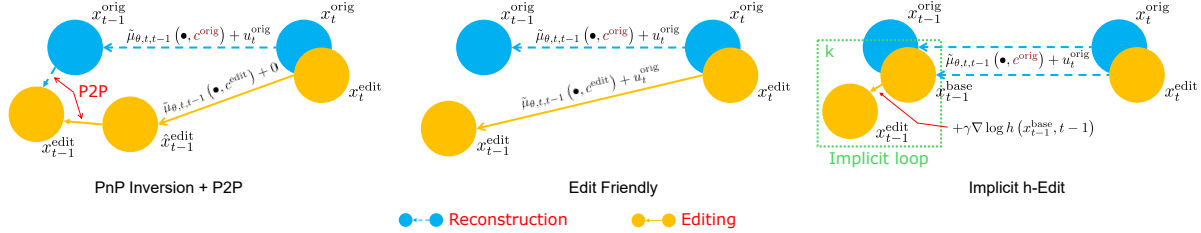


Figure 2. Overview of implicit h -Edit in comparison with PnP Inversion + P2P [27] and Edit Friendly [24].

Corollary 1. $p^h(x_0)$ is proportional to $p(x_0)p_Y(x_0)$.

Corollary 1 implies that generated samples from the bridge not only possess the attributes \mathcal{Y} but also look real. The realism associated with $p(x_0)$ comes from the base process used to construct the bridge. It can be suppressed if $h(x_0, 0)$ is set to $p_Y(x_0)/p(x_0)$, resulting in $p^h(x_0) \propto p_Y(x_0)$. More generally, we can specify *any* target distribution for the bridge to converge to by appropriately selecting $h(x_0, 0)$. This highlights the generalizability of our framework for editing.

A notable special case of our framework is when $h(x_0, 0) = p(y|x_0)$ with y being a known attribute (e.g., a class label [12] or a text prompt [55]). In this case, $h(x_t, t) = \mathbb{E}_{p(x_0|x_t)}[p(y|x_0)] = p(y|x_t)$. Below, we discuss the continuous-time formulation of the bridge for the sake of completeness.

Proposition 2. If the base Markov process is characterized by the reverse-time SDE $dx_t = (f(x_t, t) - g(t)^2 \nabla \log p_t(x_t)) dt + g(t) d\bar{w}_t$ [1, 66], then the bridge constructed from it via Doob’s h -transform has the formula:

$$dx_t = \left(f(x_t, t) - g(t)^2 (\nabla \log p(x_t) + \nabla \log h(x_t, t)) \right) dt + g(t) d\bar{w}_t \quad (12)$$

3.2. h -Edit

After constructing the bridge, image editing can be carried out through ancestral sampling from time T to time 0 along the bridge. However, for a general function h , $p^h(x_{t-1}|x_t)$ is typically non-Gaussian, making direct Monte Carlo sampling from this distribution impractical. Therefore, we must rely on Markov Chain Monte Carlo (MCMC) methods, such as Langevin Monte Carlo (LMC) [53, 74], for sampling. LMC is particularly well-suited for diffusion models due to the availability of score functions at every time t .

To sample from the (unnormalized) target distribution $p^h(x_0) \propto p(x_0)h(x_0, 0)$, we perform a sequence of LCM

updates, with each update defined as follows:

$$x_{t-1} \approx x_t + \eta \nabla_{x_t} \log(p(x_t)h(x_t, t)) + \sqrt{2\eta}z \quad (13)$$

$$= \left(x_t + \eta \nabla_{x_t} \log p(x_t) + \sqrt{2\eta}z \right) + \eta \nabla_{x_t} \log h(x_t, t) \quad (14)$$

$$= \underbrace{x_{t-1}^{\text{base}}}_{\text{rec.}} + \underbrace{\eta \nabla_{x_t} \log h(x_t, t)}_{\text{editing}} \quad (15)$$

where $z \sim \mathcal{N}(0, I)$, $\eta > 0$ is the step size, x_t and x_{t-1} denote *edited* samples at time t and $t-1$, respectively. A similar expression to Eq. 15 can be derived by solving the bridge SDE in Eq. 12 using the Euler-Maruyama method [51]. Intuitively, x_{t-1} and x_{t-1}^{base} can be regarded as samples from $p^h(x_{t-1}|x_t)$ and $p(x_{t-1}|x_t)$, respectively. According to the formula of $p^h(x_{t-1}|x_t)$ in Eq. 9, we can also sample x_{t-1} as follows:

$$x_{t-1} \approx x_{t-1}^{\text{init}} + \gamma \nabla_{x_{t-1}} \log p^h(x_{t-1}|x_t) + \sqrt{2\gamma}z \quad (16)$$

$$= \left(x_{t-1}^{\text{init}} + \gamma \nabla_{x_{t-1}} \log p(x_{t-1}|x_t) + \sqrt{2\gamma}z \right) + \gamma \nabla_{x_{t-1}} \log h(x_{t-1}, t-1) \quad (17)$$

$$\approx \underbrace{x_{t-1}^{\text{base}}}_{\text{rec.}} + \underbrace{\gamma \nabla_{x_{t-1}} \log h(x_{t-1}^{\text{base}}, t-1)}_{\text{editing}} \quad (18)$$

Here, $\gamma > 0$ is the step size. The gradient $\nabla_{x_{t-1}} \log p^h(x_{t-1}|x_t)$ does not involve $h(x_t, t)$ because it is constant w.r.t. x_{t-1} . Both updates in Eqs. 15, 18 inherently fulfill two key image editing objectives - faithfulness and effectiveness - through their decomposition into a “reconstruction” term x_{t-1}^{base} and an “editing” term $\nabla_{x_t} \log h(x_t, t)$ or $\nabla_{x_{t-1}} \log h(x_{t-1}^{\text{base}}, t-1)$, with η or γ serving as the trade-off coefficient. Eq. 15 is explicit while Eq. 18 is implicit. Furthermore, we can view Eq. 18 as a general optimization problem:

$$x_{t-1} = \underset{x'_{t-1}}{\text{argmax}} \gamma \log h(x'_{t-1}, t-1) \quad (19)$$

with x_{t-1}^{base} being the initial value, and perform multiple gradient ascent updates to improve the editing quality:

$$x_{t-1}^{(0)} = x_{t-1}^{\text{base}} \quad (20)$$

$$x_{t-1}^{(k+1)} = x_{t-1}^{(k)} + \gamma \nabla_{x_{t-1}} \log h(x_{t-1}^{(k)}, t-1) \quad (21)$$

Eq. 21 is indeed the k -th iterations of the implicit update formula in Eq. 18.

We refer to our proposed editing method as ***h-Edit*** with Eqs. 15 and 18 representing the *explicit* and *implicit* versions of *h-Edit*, respectively. *h-Edit* is highly *flexible* as it can incorporate *arbitrary* log *h*-functions, provided their gradients w.r.t. noisy samples can be efficiently computed.

For text-guided editing with Stable Diffusion [55], an *explicit h-Edit* update is given by:

$$x_{t-1}^{\text{base}} = \tilde{\mu}_{\theta, \omega, t, t-1}(x_t^{\text{edit}}, c^{\text{orig}}) + u_t^{\text{orig}} \quad (22)$$

$$x_{t-1}^{\text{edit}} = x_{t-1}^{\text{base}} + \left(\sqrt{\sigma_{t-1}^2 - \omega_{t,t-1}^2 - \frac{\sigma_t a_{t-1}}{a_t}} \right) f(x_t^{\text{edit}}, t) \quad (23)$$

where $\tilde{\mu}_{\theta, \omega, t, t-1}(\cdot, \cdot)$ and u_t^{orig} are defined in Eq. 4 and Eq. 6, respectively. $f(x_t, t)$ is expressed as follows:

$$f(x_t, t) = w^{\text{edit}} \epsilon_{\theta}(x_t, t, c^{\text{edit}}) - \hat{w}^{\text{orig}} \epsilon_{\theta}(x_t, t, c^{\text{orig}}) + (\hat{w}^{\text{orig}} - w^{\text{edit}}) \epsilon_{\theta}(x_t, t, \emptyset) \quad (24)$$

Here, w^{edit} , \hat{w}^{orig} are guidance weights. \hat{w}^{orig} may differ from w^{orig} used during inversion. An *one-step implicit h-Edit* update can be derived from Eq. 23 by replacing $f(x_t^{\text{edit}}, t)$ with $f(x_{t-1}^{\text{base}}, t-1)$, which gives:

$$x_{t-1}^{\text{edit}} = x_{t-1}^{\text{base}} + \left(\sqrt{\sigma_{t-1}^2 - \omega_{t,t-1}^2 - \frac{\sigma_t a_{t-1}}{a_t}} \right) f(x_{t-1}^{\text{base}}, t-1) \quad (25)$$

A detailed derivation of Eqs. 22-25 is provided in Appdx. A.3. An overview of our method in comparison with Edit Friendly [24] and PnP Inversion [27] is shown in Fig. 2.

Next, we will delve into the design of h and its score. We will focus on the implicit form and write $\nabla \log h(x_{t-1}, t-1)$ instead of $\nabla_{x_{t-1}} \log h(x_{t-1}, t-1)$ for simplicity.

3.3. Designing *h*-Functions

3.3.1 *h*-functions for conditional diffusion models

In most conditional diffusion models, $h(x_{t-1}, t-1) = p(y|x_{t-1})$ where y is a *predefined* condition. This means:

$$\begin{aligned} \nabla \log h(x_{t-1}, t-1) &= \nabla \log p(y|x_{t-1}) \end{aligned} \quad (26)$$

$$= \nabla \log p(x_{t-1}|y) - \nabla \log p(x_{t-1}) \quad (27)$$

Eqs. 26 and 27 correspond to the classifier-based guidance and classifier-free guidance cases, respectively. For text-guided editing with SD, $\nabla \log p(x_{t-1}|y)$ and $\nabla \log p(x_{t-1})$ are modeled as $\frac{-\tilde{\epsilon}_{\theta}(x_{t-1}, t-1, c^{\text{edit}})}{\sigma_{t-1}}$ and $\frac{-\tilde{\epsilon}_{\theta}(x_{t-1}, t-1, c^{\text{orig}})}{\sigma_{t-1}}$, respectively.

3.3.2 External reward models $h(x_0, 0)$

In many practical editing scenarios, only external reward models on clean data $h(x_0, 0)$ are available. This means $h(x_t, t)$ cannot take x_t as the direct input but must be computed through $h(x_0, 0)$ as $\mathbb{E}_{p(x_0|x_t)}[h(x_0, 0)]$. Since directly sampling from $p(x_0|x_t)$ is difficult, existing works [2, 9, 79] usually approximate $h(x_t, t) = \mathbb{E}_{p(x_0|x_t)}[h(x_0, 0)]$ by $h(x_{0|t}, 0)$ where $x_{0|t} := \mathbb{E}_{p(x_0|x_t)}[x_0]$ denotes the posterior estimation of x_0 given x_t . In SD, $x_{0|t}$ can be derived from x_t and $\tilde{\epsilon}_{\theta}(x_t, t, c^{\text{orig}})$ as $\frac{x_t - \sigma_t \tilde{\epsilon}_{\theta}(x_t, t, c^{\text{orig}})}{a_t}$ based on Tweedie’s formula [16].

3.3.3 *h*-functions for reconstruction

In addition to using h as an editing function, we can design an *h*-function specifically for reconstruction, defined as:

$$h_{\text{rec}}(x_{t-1}, t-1) := \exp\left(-\lambda_{t-1} \|x_{t-1} - x_{t-1}^{\text{base}}\|_2^2\right) \quad (28)$$

When this *h*-function is integrated into our optimization framework in Eq. 19, it enables simultaneous optimization-free and optimization-based reconstruction (via x_{t-1}^{base} and $\nabla \log h_{\text{rec}}(x_{t-1}, t-1)$, respectively), exclusive to *h-Edit*.

3.3.4 Product of *h*-Experts

Since $\log h$ can be interpreted as a *negative energy function*, we can combine multiple *h*-functions to create a “product of *h*-experts” as follows:

$$h = h_1 * h_2 * \dots * h_m \quad (29)$$

where m denotes the number of *h*-functions. The combined *h*-function in Eq. 29 can be easily integrated into our framework by summing the score for each component:

$$\nabla \log h(x_{t-1}, t-1) = \sum_{i=1}^m \nabla \log h_i(x_{t-1}, t-1) \quad (30)$$

4. Related Work

Due to space constraints, this section only covers related work in training-free editing. For details on conditional generation and diffusion bridges, please refer to Appdx. C.

The advent of conditional diffusion models, particularly text-guided latent diffusion models like Stable Diffusion [55], has greatly advanced the development of various diffusion-based text-guided image editing techniques. These methods can be broadly categorized into training-based [31, 33, 35, 82] and training-free methods [38, 44, 46, 76, 77]. Unlike training-based methods, which finetune the noise network [33] or employ an auxiliary model [35] through additional training, training-free methods modify

| Inv. | Attn. | Method | CLIP Sim. \uparrow | Local CLIP \uparrow | DINO Dist. $\times 10^2\downarrow$ | LPIPS $\times 10^2\downarrow$ | SSIM $\times 10\uparrow$ | PSNR \uparrow |
|--------|-------|------------------|----------------------|-----------------------|------------------------------------|-------------------------------|--------------------------|-----------------|
| Deter. | P2P | NP | 0.246 | <u>0.140</u> | 1.62 | 6.90 | 8.34 | 26.21 |
| | | NT | 0.248 | <u>0.130</u> | 1.34 | 6.07 | 8.41 | 27.03 |
| | | StyleD | 0.248 | 0.085 | 1.17 | 6.61 | 8.34 | 26.05 |
| | | NMG | 0.249 | 0.087 | <u>1.32</u> | 5.59 | 8.47 | 27.05 |
| | | PnP Inv | <u>0.250</u> | 0.095 | 1.17 | <u>5.46</u> | <u>8.48</u> | <u>27.22</u> |
| | | <i>h</i> -Edit-D | 0.253 | 0.147 | 1.17 | 4.85 | 8.54 | 27.87 |
| Random | None | EF | <u>0.254</u> | <u>0.122</u> | <u>1.29</u> | <u>6.09</u> | <u>8.37</u> | <u>25.87</u> |
| | | LEDITS++ | 0.254 | <u>0.113</u> | 2.34 | 8.88 | 8.11 | 23.36 |
| | | <i>h</i> -Edit-R | 0.255 | 0.148 | 1.28 | 5.55 | 8.46 | 26.43 |
| | P2P | EF | 0.255 | 0.126 | 1.51 | 5.70 | 8.40 | 26.30 |
| | | <i>h</i> -Edit-R | 0.256 | 0.159 | 1.45 | 5.08 | 8.50 | 26.97 |

Table 1. Text-guided image editing results of *h*-Edit and other baselines. The best and second best results for each metric and inversion type are highlighted in bold and underscored, respectively.

the attention or feature maps in Stable Diffusion (SD) [6, 19, 50, 70] or adjust the generation process of SD [46] to ensure editing fidelity. Null-text inversion (NTI) [46] optimizes the null-text embedding during generation to minimize discrepancies between this process and the forward process. Prompt Tuning inversion (PTI) [14] interpolates between the target text embedding and the null-text embedding optimized by NTI to create a more suitable embedding for editing. EDICT [72] draws inspiration from affine coupling layers in normalizing flows to design a more faithful reconstruction process compared to DDIM sampling. Negative Prompt inversion (NPI) [45] bypasses the costly optimization of NTI by using the original text embedding instead of the null-text embedding, while ProxNPI [18] adds an auxiliary regularization term to enhance NPI’s reconstruction capabilities. Noise Map Guidance (NMG) [7] leverages energy-based guidance [83] and information from the inversion process to denoise samples in a way that improve reconstruction. PnP Inversion [27] avoids optimization by incorporating the difference between inversion and reconstruction samples directly into the editing update. AIDI [48] views exact reconstruction as a fixed-point iteration problem and use Anderson acceleration to find the solution. Unlike these deterministic-inversion-based methods, Edit Friendly (EF) [24] employs random inversion with independent sampling of intermediate noisy samples, achieving good reconstruction without the need for attention map adjustments like P2P. LEDITS++ [3] introduces several enhancements to EF, improving both efficiency and versatility in editing. Generally, most training-free methods are limited to text-guided editing, while our approach allows for the seamless combination of multiple editing types due to the clear separation of the reconstruction and editing terms.

5. Experiments

Due to space limit, we only provide main results in this section and refer readers to Appdx. F for our ablation studies on w^{edit} , \hat{w}^{orig} , the number of optimization steps, as well as

other additional results.

5.1. Text-guided Editing

5.1.1 Experiment Setup

We evaluate our method on text-guided image editing using the PIE-Bench dataset [27], which includes 700 diverse images of humans, animals, and objects across various environments. Each image comes with an original and edited text descriptions and an annotated mask indicating the editing region. PIE-Bench features 10 distinct editing categories, including adding, removing, or modifying objects, styles, and backgrounds.

For evaluation, we follow [27] to use CLIP similarity [52] between the edited image and text to measure editing effectiveness. To assess editing faithfulness, we compute PSNR, LPIPS [81], and SSIM [73] on non-edited regions, as defined by the editing masks, and DINO feature distance [69] on the entire image. Additionally, we include local directional CLIP similarity [33] to enhance evaluation of editing effectiveness, as standard CLIP similarity may be insufficient when the edited attribute represents only a small part of the target text. While these metrics offer insights, they are imperfect, as analyzed in Appdx. G. Visual assessments remain essential for evaluating editing quality.

We compare *h*-Edit with state-of-the-art diffusion-based text-guided editing baselines that use either deterministic or random inversion, including NT [46], NP [45], StyleD [38], NMG [7], PnP Inv [27], EF [24], and LEDITS++ [3]. We refer to *h*-Edit with deterministic inversion as *h*-Edit-D, and with random inversion as *h*-Edit-R. For a fair comparison, we adhere to the default settings in [24, 27], using Stable Diffusion v1.4 [55] and 50 sampling steps for editing. Following [27], we apply Prompt-to-Prompt (P2P) [19] to all deterministic-inversion-based methods to ensure faithful reconstruction. For random-inversion-based methods, we report results both with and without P2P. Unless otherwise specified, we use the implicit form with a single optimization step (Eq. 18) for both *h*-Edit-D and *h*-Edit-R. The hy-



| Method | ID↑ | Expr.↓ | Pose↓ | LPIPS↓ | FID↓ |
|-----------------------|-------------|-------------|-------------|-------------|--------------|
| FaceShifter | 0.70 | 2.39 | 2.81 | 0.08 | 10.16 |
| MegaFS | 0.34 | 2.88† | 7.71 | 0.15 | 27.07 |
| AFS | 0.47 | 2.92 | 4.68 | 0.13 | 17.55 |
| DiffFace | 0.61 | 3.04 | 4.35 | 0.10 | <u>11.89</u> |
| EF | 0.74 | 3.10 | 4.12 | 0.06 | 20.78 |
| <i>h</i> -edit-R | <u>0.80</u> | <u>2.76</u> | <u>3.78</u> | 0.04 | 17.68 |
| <i>h</i> -edit-R (3s) | 0.84 | 3.10 | 4.29 | <u>0.05</u> | 19.12 |

Figure 3. **Left:** Visualization of swapped faces produced by implicit *h*-Edit-R and baselines. (3s) denotes *h*-Edit-R with 3 optimization steps. Identity similarity scores (higher is better) are displayed below each output. **Right:** Face swapping results of implicit *h*-Edit-R and other baselines. †: The expression error for MegaFS was calculated on images with detectable faces, as required by the evaluation metric.

perparameters w^{orig} , w^{edit} , \hat{w}^{orig} are set to 1.0, 10.0, 9.0 for *h*-Edit-D, and 1.0, 7.5, 5.0 for *h*-Edit-R, respectively, as these values yield strong quantitative and qualitative results. Detailed ablation studies on these hyperparameters are provided in Appdx. F.

5.1.2 Results

As shown in Table 1, *h*-Edit-D + P2P significantly outperforms all deterministic-inversion-based baselines with P2P in both editing effectiveness and faithfulness. For example, our method improves over NT, a strong baseline, by 1.22×10^{-2} in LPIPS and 0.017 in local CLIP similarity. We observed that PnP Inv and NMG often reconstruct the original image in challenging editing scenarios, achieving high faithfulness despite not actually making meaningful changes. In contrast, *h*-Edit-D + P2P consistently performs successful edits while maintaining superior faithfulness. This validates the theoretical soundness of *h*-Edit compared to other methods.

Similarly, *h*-Edit-R outperforms both EF and LEDITS++ across all metrics, with or without P2P. This improvement is largely due to the implicit form and the carefully selected value of \hat{w}^{orig} - features unique to *h*-Edit. Additionally, we observed that LEDITS++ occasionally produces unfaithful or erroneous images, even after hyperparameter tuning. Notably, random-inversion methods (including *h*-Edit-R) without P2P often fall behind their P2P-enabled counterparts in changing color and texture but excel in adding and removing objects, suggesting that the choice to combine with P2P depends on the specific editing scenario.

In Fig. 1 and Appdx. E.1, we provide a *non-exhaustive* list of edited images by our method and baselines, showcasing our superior performance.

5.2. Face Swapping

5.2.1 Experimental Settings

We consider face swapping as a benchmark to verify the capabilities of *h*-Edit in reward-model-based editing. Given a diffusion model trained on 256×256 CelebA-HQ facial images [28, 44], and a pretrained ArcFace model [11], our goal is to transfer the identity from a reference face x_0^{ref} to an original face x_0^{orig} while preserving other attributes of x_0^{orig} such as hair style, pose, facial expression, and background. For this experiment, we use 5,000 pairs $(x_0^{\text{orig}}, x_0^{\text{ref}})$ sampled randomly from CelebA-HQ.

We use implicit *h*-Edit-R with either 1 or 3 optimization steps. Since P2P is inapplicable to unconditional diffusion models, our method operates without P2P. The cosine similarity between the edited image x_0^{edit} and x_0^{ref} is employed as the reward, and the score $\nabla \log h(x_{t-1}, t-1)$ is approximated based on the technique discussed in Section 3.3.2. We compare *h*-Edit-R to well-known face-swapping methods, including GAN-based (FaceShifter [37]), Style-GAN-based (MegaFS [86] and AFS [71]), and diffusion-based (DiffFace [34]). Unlike DiffFace which is a training based method, our method is training-free. We also include EF as a training-free baseline by adding the score to its editing term as described in Algo. B.2. This extension of EF has never been considered in the literature. We use 100 sampling steps for all diffusion-based methods, including DiffFace. Facial images generated by all methods are masked before evaluation, with unmasked results provided in Appdx. F.5. Following [37, 71], we assess editing effectiveness via cosine similarity using ArcFace, faithfulness via expression/pose error and LPIPS, and visual quality via FID [20].

5.2.2 Results

As shown in Fig. 3 (right), both versions of *h*-Edit-R achieve the highest face-swapping accuracies. *h*-Edit-R also ranks second-best in preserving expressions and poses,

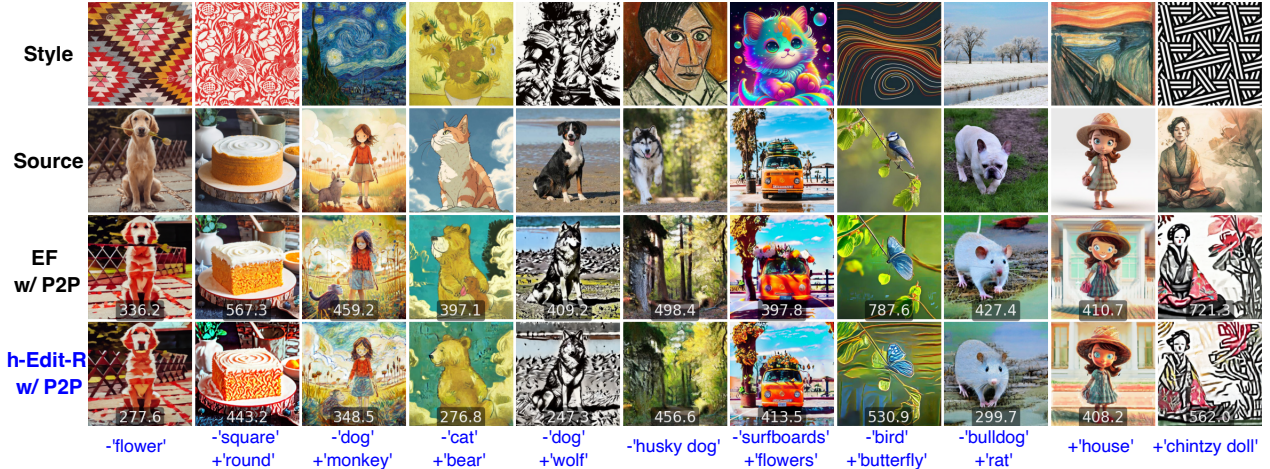


Figure 4. Qualitative comparison of h -Edit-R + P2P and EF + P2P in the combined editing task. Style losses (lower is better) are shown below each output image. h -Edit-R + P2P achieves superior results in both style transfer and text-guided editing.

outperforming DiffFace and EF by large margins. However, in terms of FID, our method falls short of FaceShifter and DiffFace, likely because these methods are specifically tailored for face swapping and trained on larger face datasets (FFHQ [29] for DiffFace and FFHQ + CelebA-HQ for FaceShifter). Using three optimization steps improves the identity transfer accuracy compared to using one both quantitatively and qualitatively (Fig. 3 (left)), showcasing the advantage of our implicit form. However, this improvement may slightly reduce faithfulness, especially when the source and reference faces differ significantly. Additional visualizations are provided in Appdx. E.2.

5.3. Combined Text-guided and Style Editing

5.3.1 Experimental Settings

This task is similar to text-guided editing in Section 5.1 but with an additional requirement: the edited image x_0^{edit} should have similar style as a reference image x_0^{sty} . Following [79], we use the negative L2 distance between the Gram matrices [26] from the third feature layer of the CLIP image encoder w.r.t. x_0^{edit} and x_0^{sty} as a style reward. The norm of the style reward score is scaled to match the norm of the editing function $f(\cdot)$ in Eq. 24 at each time t , inspired by [79]. In this experiment, each original image x_0^{orig} from the PIE-Bench dataset is paired with a style image randomly selected from a set of 11 styles shown in Fig. 4. We employ implicit h -Edit-R + P2P and compare it with EF + P2P. We keep $(w^{\text{edit}}, \hat{w}^{\text{orig}})$ for our method and w^{edit} for EF the same as in Section 5.1, tuning only the style editing coefficient ρ^{sty} . Given the limitations of existing metrics in evaluating stylized edited images, our choice of ρ^{sty} is based primarily on visual quality. We found that ρ^{sty} equal 0.6 and 1.5 provide the best results for our method and EF, respectively.

Additional justification for this selection is provided in Appdx. E.3. All other settings remain consistent with those used in the text-guided editing experiment.

5.3.2 Results

It can be seen from Fig. 4 and the visualizations in Appdx. E.3 that h -Edit-R + P2P achieves more effective text-guided and style edits while better preserving non-edited content compared to EF + P2P. EF + P2P seems to struggle with combined editing task, sometimes introducing artifacts (e.g., a baby bear in the fourth column in Fig. 4) or altering non-edited content (e.g., a different girl in the third column). Additionally, EF + P2P is more sensitive to the change of ρ^{sty} as slightly increasing ρ^{sty} can improve style editing but also exacerbate the unfaithfulness problem (Appdx. E.3).

6. Conclusion

We introduced the reverse-time bridge modeling framework for effective diffusion-based image editing, and proposed h -Edit - a novel training-free editing method - as an instance of our framework. h -Edit leverages Doob’s h -transform and Langevin Monte Carlo to create an effective editing update, composed of the “reconstruction” and “editing” terms, which capture the editing faithfulness and effectiveness, respectively. This design grants our method great flexibility, allowing for seamless integration of various h -functions to support different editing objectives. Extensive experiments across diverse editing tasks demonstrated that h -Edit achieves state-of-the-art editing performance, as evidenced by quantitatively and qualitatively metrics. These results validate both the theoretical soundness and practical strength of our method, which we hope will inspire future

research to address more complex real-world editing challenges while maintaining theoretical guarantees.

Despite these advantages, our method faces challenges in some difficult editing cases. Although these issues could be partially mitigated by using the implicit version with multiple optimization loops (Appdx. F.3) or by manually increasing w^{edit} and \hat{w}^{orig} (Appdx. F.1), an automated solution for handling them would be highly beneficial. Another promising direction is to modify x_{t-1}^{base} to focus on preserving only the non-edited regions, enhancing editing effectiveness.

Acknowledgement

The experiments in this research were partially supported by AWS Cloud services under the AWS Cloud Credit for Research Program, for which Dr. Kien Do is the recipient.

References

- [1] Brian DO Anderson. Reverse-time diffusion equation models. *Stochastic Processes and their Applications*, 12(3):313–326, 1982. 4
- [2] Arpit Bansal, Hong-Min Chu, Avi Schwarzschild, Soumyadip Sengupta, Micah Goldblum, Jonas Geiping, and Tom Goldstein. Universal guidance for diffusion models. In *ICLR*, 2024. 5, 20
- [3] Manuel Brack, Felix Friedrich, Katharia Kornmeier, Linoy Tsaban, Patrick Schramowski, Kristian Kersting, and Apolinário Passos. Ledits++: Limitless image editing using text-to-image models. In *CVPR*, pages 8861–8870, 2024. 6, 20
- [4] Tim Brooks, Aleksander Holynski, and Alexei A Efros. Instructpix2pix: Learning to follow image editing instructions. In *CVPR*, pages 18392–18402, 2023. 19
- [5] Tom Brown, Benjamin Mann, Nick Ryder, Melanie Subbiah, Jared D Kaplan, Prafulla Dhariwal, Arvind Neelakantan, Pranav Shyam, Girish Sastry, Amanda Askell, Sandhini Agarwal, Ariel Herbert-Voss, Gretchen Krueger, Tom Henighan, Rewon Child, Aditya Ramesh, Daniel Ziegler, Jeffrey Wu, Clemens Winter, Chris Hesse, Mark Chen, Eric Sigler, Mateusz Litwin, Scott Gray, Benjamin Chess, Jack Clark, Christopher Berner, Sam McCandlish, Alec Radford, Ilya Sutskever, and Dario Amodei. Language models are few-shot learners. In *NeurIPS*, pages 1877–1901. Curran Associates, Inc., 2020. 19
- [6] Mingdeng Cao, Xintao Wang, Zhongang Qi, Ying Shan, Xiaohu Qie, and Yinqiang Zheng. Masactrl: Tuning-free mutual self-attention control for consistent image synthesis and editing. In *ICCV*, pages 22560–22570, 2023. 6, 24, 25
- [7] Hansam Cho, Jonghyun Lee, Seoung Bum Kim, Tae-Hyun Oh, and Yonghyun Jeong. Noise map guidance: Inversion with spatial context for real image editing. In *ICLR*, 2024. 2, 6, 21
- [8] Jooyoung Choi, Sungwon Kim, Yonghyun Jeong, Youngjune Gwon, and Sungroh Yoon. Ilvr: Conditioning method for denoising diffusion probabilistic models. In *ICCV*, pages 14367–14376, 2021. 1
- [9] Hyungjin Chung, Jeongsol Kim, Michael T Mccann, Marc L Klasky, and Jong Chul Ye. Diffusion posterior sampling for general noisy inverse problems. In *ICLR*. The International Conference on Learning Representations, 2023. 5, 20
- [10] Valentin De Bortoli, James Thornton, Jeremy Heng, and Arnaud Doucet. Diffusion schrödinger bridge with applications to score-based generative modeling. *NeurIPS*, 34:17695–17709, 2021. 3, 20
- [11] Jiankang Deng, Jia Guo, Niannan Xue, and Stefanos Zafeiriou. Arcface: Additive angular margin loss for deep face recognition. In *CVPR*, pages 4690–4699, 2019. 7
- [12] Prafulla Dhariwal and Alexander Nichol. Diffusion models beat gans on image synthesis. *NeurIPS*, 34: 8780–8794, 2021. 1, 2, 4, 20
- [13] Kien Do, Duc Kieu, Toan Nguyen, Dang Nguyen, Hung Le, Dung Nguyen, and Thin Nguyen. Variational flow models: Flowing in your style. *arXiv preprint arXiv:2402.02977*, 2024. 28
- [14] Wenkai Dong, Song Xue, Xiaoyue Duan, and Shumin Han. Prompt tuning inversion for text-driven image editing using diffusion models. In *ICCV*, pages 7430–7440, 2023. 3, 6
- [15] Joseph L Doob and JI Doob. *Classical potential theory and its probabilistic counterpart*. Springer, 1984. 2, 3, 20
- [16] Bradley Efron. Tweedie’s formula and selection bias. *Journal of the American Statistical Association*, 106 (496):1602–1614, 2011. 5, 20
- [17] Rinon Gal, Or Patashnik, Haggai Maron, Amit H Bermano, Gal Chechik, and Daniel Cohen-Or. Stylegan-nada: Clip-guided domain adaptation of image generators. *ACM Transactions on Graphics (TOG)*, 41(4):1–13, 2022. 19
- [18] Ligong Han, Song Wen, Qi Chen, Zhixing Zhang, Kunpeng Song, Mengwei Ren, Ruijiang Gao, Anastasis Stathopoulos, Xiaoxiao He, Yuxiao Chen, et al. Proxedit: Improving tuning-free real image editing with proximal guidance. In *WACV*, pages 4291–4301, 2024. 6
- [19] Amir Hertz, Ron Mokady, Jay Tenenbaum, Kfir Aberman, Yael Pritch, and Daniel Cohen-or. Prompt-to-prompt image editing with cross-attention control. In *ICLR*, 2023. 1, 2, 3, 6, 17, 18, 19, 24
- [20] Martin Heusel, Hubert Ramsauer, Thomas Unterthiner, Bernhard Nessler, and Sepp Hochreiter.

- Gans trained by a two time-scale update rule converge to a local nash equilibrium. *NIPS*, 30, 2017. 7
- [21] Jonathan Ho and Tim Salimans. Classifier-free diffusion guidance. *arXiv preprint arXiv:2207.12598*, 2022. 1, 2, 20
- [22] Jonathan Ho, Ajay Jain, and Pieter Abbeel. Denoising diffusion probabilistic models. *NeurIPS*, 33:6840–6851, 2020. 1, 2, 20
- [23] Yi Huang, Jiancheng Huang, Yifan Liu, Mingfu Yan, Jiayi Lv, Jianzhuang Liu, Wei Xiong, He Zhang, Shifeng Chen, and Liangliang Cao. Diffusion model-based image editing: A survey. *arXiv preprint arXiv:2402.17525*, 2024. 1
- [24] Inbar Huberman-Spiegelglas, Vladimir Kulikov, and Tomer Michaeli. An edit friendly ddpn noise space: Inversion and manipulations. In *CVPR*, pages 12469–12478, 2024. 2, 3, 4, 5, 6, 19, 20
- [25] Aapo Hyvärinen and Peter Dayan. Estimation of non-normalized statistical models by score matching. *Journal of Machine Learning Research*, 6(4), 2005. 20
- [26] Justin Johnson, Alexandre Alahi, and Li Fei-Fei. Perceptual losses for real-time style transfer and super-resolution. In *ECCV*, pages 694–711. Springer, 2016. 8
- [27] Xuan Ju, Ailing Zeng, Yuxuan Bian, Shaoteng Liu, and Qiang Xu. Pnp inversion: Boosting diffusion-based editing with 3 lines of code. *ICLR*, 2024. 2, 3, 4, 5, 6, 20, 21, 24
- [28] Tero Karras. Progressive growing of gans for improved quality, stability, and variation. *arXiv preprint arXiv:1710.10196*, 2017. 7
- [29] Tero Karras, Samuli Laine, and Timo Aila. A style-based generator architecture for generative adversarial networks. In *CVPR*, pages 4401–4410, 2019. 8
- [30] Jack Karush. On the chapman-kolmogorov equation. *The Annals of Mathematical Statistics*, 32(4):1333–1337, 1961. 14
- [31] Bahjat Kawar, Shiran Zada, Oran Lang, Omer Tov, Huiwen Chang, Tali Dekel, Inbar Mosseri, and Michal Irani. Imagic: Text-based real image editing with diffusion models. In *CVPR*, pages 6007–6017, 2023. 5
- [32] Duc Kieu, Kien Do, Toan Nguyen, Dang Nguyen, and Thin Nguyen. Bidirectional diffusion bridge models. *arXiv preprint arXiv:2502.09655*, 2025. 3, 14
- [33] Gwanghyun Kim, Taesung Kwon, and Jong Chul Ye. Diffusionclip: Text-guided diffusion models for robust image manipulation. In *CVPR*, pages 2426–2435, 2022. 5, 6, 19
- [34] Kihong Kim, Yunho Kim, Seokju Cho, Junyoung Seo, Jisu Nam, Kychul Lee, Seungryong Kim, and KwangHee Lee. Diffface: Diffusion-based face swapping with facial guidance. *arXiv preprint arXiv:2212.13344*, 2022. 7
- [35] Mingi Kwon, Jaeseok Jeong, and Youngjung Uh. Diffusion models already have a semantic latent space. In *ICLR*, 2023. 5, 19
- [36] Bo Li, Kaitao Xue, Bin Liu, and Yu-Kun Lai. Bbim: Image-to-image translation with brownian bridge diffusion models. In *CVPR*, pages 1952–1961, 2023. 3
- [37] Lingzhi Li, Jianmin Bao, Hao Yang, Dong Chen, and Fang Wen. Advancing high fidelity identity swapping for forgery detection. In *CVPR*, pages 5074–5083, 2020. 7, 28
- [38] Senmao Li, Joost van de Weijer, Taihang Hu, Fahad Shahbaz Khan, Qibin Hou, Yaxing Wang, and Jian Yang. Stylediffusion: Prompt-embedding inversion for text-based editing. *arXiv preprint arXiv:2303.15649*, 2023. 3, 5, 6, 21
- [39] Guan-Hong Liu, Arash Vahdat, De-An Huang, Evangelos A Theodorou, Weili Nie, and Anima Anandkumar. I2sb: image-to-image schrödinger bridge. In *ICML*, pages 22042–22062, 2023. 3, 20
- [40] Nan Liu, Shuang Li, Yilun Du, Antonio Torralba, and Joshua B Tenenbaum. Compositional visual generation with composable diffusion models. In *ECCV*, pages 423–439. Springer, 2022. 20
- [41] Xingchao Liu and Lemeng Wu. Learning diffusion bridges on constrained domains. In *ICLR*, 2023. 3, 20
- [42] Xingchao Liu, Lemeng Wu, Mao Ye, and Qiang Liu. Let us build bridges: Understanding and extending diffusion generative models. *arXiv preprint arXiv:2208.14699*, 2022. 3
- [43] Cheng Lu, Yuhao Zhou, Fan Bao, Jianfei Chen, Chongxuan Li, and Jun Zhu. Dpm-solver++: Fast solver for guided sampling of diffusion probabilistic models. *arXiv preprint arXiv:2211.01095*, 2022. 28
- [44] Chenlin Meng, Yutong He, Yang Song, Jiaming Song, Jiajun Wu, Jun-Yan Zhu, and Stefano Ermon. SDEdit: Guided image synthesis and editing with stochastic differential equations. In *ICLR*, 2022. 1, 5, 7
- [45] Daiki Miyake, Akihiro Iohara, Yu Saito, and Toshiyuki Tanaka. Negative-prompt inversion: Fast image inversion for editing with text-guided diffusion models. *arXiv preprint arXiv:2305.16807*, 2023. 6, 21
- [46] Ron Mokady, Amir Hertz, Kfir Aberman, Yael Pritch, and Daniel Cohen-Or. Null-text inversion for editing real images using guided diffusion models. In *CVPR*, pages 6038–6047, 2023. 2, 3, 5, 6, 21
- [47] Alexander Quinn Nichol, Prafulla Dhariwal, Aditya Ramesh, Pranav Shyam, Pamela Mishkin, Bob McGrew, Ilya Sutskever, and Mark Chen. Glide: Towards photorealistic image generation and editing with text-guided diffusion models. In *ICML*, pages 16784–16804. PMLR, 2022. 1

- [48] Zhihong Pan, Riccardo Gherardi, Xiufeng Xie, and Stephen Huang. Effective real image editing with accelerated iterative diffusion inversion. In *ICCV*, pages 15912–15921, 2023. 6
- [49] Omkar Parkhi, Andrea Vedaldi, and Andrew Zisserman. Deep face recognition. In *BMVC*. British Machine Vision Association, 2015. 21
- [50] Gaurav Parmar, Krishna Kumar Singh, Richard Zhang, Yijun Li, Jingwan Lu, and Jun-Yan Zhu. Zero-shot image-to-image translation. In *ACM SIGGRAPH*, pages 1–11, 2023. 6
- [51] Eckhard Platen Peter E. Kloeden. *Numerical Solution of Stochastic Differential Equations*. Springer-Verlag, 1992. 4
- [52] Alec Radford, Jong Wook Kim, Chris Hallacy, Aditya Ramesh, Gabriel Goh, Sandhini Agarwal, Girish Sastry, Amanda Askell, Pamela Mishkin, Jack Clark, et al. Learning transferable visual models from natural language supervision. In *ICML*, pages 8748–8763. PMLR, 2021. 6
- [53] Gareth O Roberts and Richard L Tweedie. Exponential convergence of langevin distributions and their discrete approximations. *Bernoulli*, 2(4):341–363, 1996. 2, 4
- [54] L Chris G Rogers and David Williams. *Diffusions, Markov processes and martingales: Volume 2, Itô calculus*. Cambridge university press, 2000. 2, 3
- [55] Robin Rombach, Andreas Blattmann, Dominik Lorenz, Patrick Esser, and Björn Ommer. High-resolution image synthesis with latent diffusion models. In *CVPR*, pages 10684–10695, 2022. 1, 2, 4, 5, 6
- [56] Chitwan Saharia, William Chan, Huiwen Chang, Chris Lee, Jonathan Ho, Tim Salimans, David Fleet, and Mohammad Norouzi. Palette: Image-to-image diffusion models. In *ACM SIGGRAPH 2022 conference proceedings*, pages 1–10, 2022. 1
- [57] Chitwan Saharia, William Chan, Saurabh Saxena, Lala Li, Jay Whang, Emily Denton, Seyed Kamyar Seyed Ghasemipour, Raphael Gontijo-Lopes, Burcu Karagol Ayan, Tim Salimans, et al. Photorealistic text-to-image diffusion models with deep language understanding. In *NeurIPS*, 2022. 1
- [58] Simo Särkkä and Arno Solin. *Applied stochastic differential equations*. Cambridge University Press, 2019. 2, 3
- [59] Florian Schroff, Dmitry Kalenichenko, and James Philbin. Facenet: A unified embedding for face recognition and clustering. In *CVPR*, pages 815–823, 2015. 21
- [60] Sefik Serengil and Alper Ozpinar. A benchmark of facial recognition pipelines and co-usability performances of modules. *Journal of Information Technologies*, 17(2):95–107, 2024. 21
- [61] Sefik Ilkin Serengil and Alper Ozpinar. Lightface: A hybrid deep face recognition framework. In *2020 Innovations in Intelligent Systems and Applications Conference (ASYU)*, pages 23–27. IEEE, 2020. 21
- [62] Jascha Sohl-Dickstein, Eric Weiss, Niru Maheswaranathan, and Surya Ganguli. Deep unsupervised learning using nonequilibrium thermodynamics. In *ICML*, pages 2256–2265. PMLR, 2015. 1, 2
- [63] Vignesh Ram Somnath, Matteo Pariset, Ya-Ping Hsieh, Maria Rodriguez Martinez, Andreas Krause, and Charlotte Bunne. Aligned diffusion schrödinger bridges. In *UAI*, pages 1985–1995. PMLR, 2023. 3, 20
- [64] Jiaming Song, Chenlin Meng, and Stefano Ermon. Denoising diffusion implicit models. In *ICLR*, 2021. 1, 2, 3
- [65] Yang Song and Stefano Ermon. Generative modeling by estimating gradients of the data distribution. *NeurIPS*, 32, 2019. 1, 2, 20
- [66] Yang Song, Jascha Sohl-Dickstein, Diederik P Kingma, Abhishek Kumar, Stefano Ermon, and Ben Poole. Score-based generative modeling through stochastic differential equations. In *ICLR*, 2021. 4
- [67] Alexander Y Tong, Nikolay Malkin, Kilian Fatras, Lazar Atanackovic, Yanlei Zhang, Guillaume Huguët, Guy Wolf, and Yoshua Bengio. Simulation-free schrödinger bridges via score and flow matching. In *AISTATS*, pages 1279–1287. PMLR, 2024. 3
- [68] Omer Tov, Yuval Alaluf, Yotam Nitzan, Or Patashnik, and Daniel Cohen-Or. Designing an encoder for stylegan image manipulation. *ACM Transactions on Graphics (TOG)*, 40(4):1–14, 2021. 20
- [69] Narek Tumanyan, Omer Bar-Tal, Shai Bagon, and Tali Dekel. Splicing vit features for semantic appearance transfer. In *CVPR*, pages 10748–10757, 2022. 6
- [70] Narek Tumanyan, Michal Geyer, Shai Bagon, and Tali Dekel. Plug-and-play diffusion features for text-driven image-to-image translation. In *CVPR*, pages 1921–1930, 2023. 2, 6, 24, 25
- [71] Truong Vu, Kien Do, Khang Nguyen, and Khoat Than. Face swapping as a simple arithmetic operation. *arXiv preprint arXiv:2211.10812*, 2022. 7, 28
- [72] Bram Wallace, Akash Gokul, and Nikhil Naik. Edict: Exact diffusion inversion via coupled transformations. In *CVPR*, pages 22532–22541, 2023. 6
- [73] Zhou Wang, Alan C Bovik, Hamid R Sheikh, and Eero P Simoncelli. Image quality assessment: from error visibility to structural similarity. *IEEE transactions on image processing*, 13(4):600–612, 2004. 6
- [74] Max Welling and Yee W Teh. Bayesian learning

- via stochastic gradient langevin dynamics. In *ICML*, pages 681–688. Citeseer, 2011. [2](#), [4](#)
- [75] Chen Henry Wu and Fernando De la Torre. A latent space of stochastic diffusion models for zero-shot image editing and guidance. In *ICCV*, pages 7378–7387, 2023. [3](#)
- [76] Qiucheng Wu, Yujian Liu, Handong Zhao, Ajinkya Kale, Trung Bui, Tong Yu, Zhe Lin, Yang Zhang, and Shiyu Chang. Uncovering the disentanglement capability in text-to-image diffusion models. In *CVPR*, pages 1900–1910, 2023. [5](#)
- [77] Sihan Xu, Yidong Huang, Jiayi Pan, Ziqiao Ma, and Joyce Chai. Inversion-free image editing with language-guided diffusion models. In *CVPR*, pages 9452–9461, 2024. [5](#)
- [78] Changqian Yu, Jingbo Wang, Chao Peng, Changxin Gao, Gang Yu, and Nong Sang. Bisenet: Bilateral segmentation network for real-time semantic segmentation. In *ECCV*, pages 325–341, 2018. [21](#)
- [79] Jiwen Yu, Yinhuai Wang, Chen Zhao, Bernard Ghanem, and Jian Zhang. Freedom: Training-free energy-guided conditional diffusion model. In *ICCV*, pages 23174–23184, 2023. [1](#), [5](#), [8](#), [19](#), [20](#), [21](#), [28](#)
- [80] Lvmin Zhang, Anyi Rao, and Maneesh Agrawala. Adding conditional control to text-to-image diffusion models. In *ICCV*, pages 3836–3847, 2023. [1](#)
- [81] Richard Zhang, Phillip Isola, Alexei A Efros, Eli Shechtman, and Oliver Wang. The unreasonable effectiveness of deep features as a perceptual metric. In *CVPR*, pages 586–595, 2018. [6](#)
- [82] Zhixing Zhang, Ligong Han, Arnab Ghosh, Dimitris N Metaxas, and Jian Ren. Sine: Single image editing with text-to-image diffusion models. In *CVPR*, pages 6027–6037, 2023. [5](#)
- [83] Min Zhao, Fan Bao, Chongxuan Li, and Jun Zhu. Egsde: Unpaired image-to-image translation via energy-guided stochastic differential equations. *NeurIPS*, 35:3609–3623, 2022. [6](#), [20](#)
- [84] Wenliang Zhao, Lujia Bai, Yongming Rao, Jie Zhou, and Jiwen Lu. Unipc: A unified predictor-corrector framework for fast sampling of diffusion models. *Advances in Neural Information Processing Systems*, 36:49842–49869, 2023. [28](#)
- [85] Linqi Zhou, Aaron Lou, Samar Khanna, and Stefano Ermon. Denoising diffusion bridge models. In *ICLR*, 2024. [3](#), [20](#)
- [86] Yuhao Zhu, Qi Li, Jian Wang, Cheng-Zhong Xu, and Zhenan Sun. One shot face swapping on megapixels. In *CVPR*, pages 4834–4844, 2021. [7](#), [28](#)

Table of Content for Appendix

| | |
|---|-----------|
| A Theoretical Results | 14 |
| A.1. Derivation of the formula of $h(x_t, t)$ | 14 |
| A.2. Proof of Proposition 1 | 14 |
| A.3. Closed-form expressions for the explicit and implicit h -Edit updates for Stable Diffusion | 15 |
| B Algorithms | 16 |
| B.1. h -Edit for Combined Editing | 16 |
| B.2. Edit Friendly for Combined Editing | 19 |
| C Additional Discussion on Related Work | 19 |
| C.1. Training-based Editing | 19 |
| C.2. Conditional Generation with Diffusion Models | 20 |
| C.3. Diffusion Bridges and Doob’s h -Transform | 20 |
| D Further Details on Experimental Settings | 20 |
| D.1. Text-guided Editing | 20 |
| D.2. Face Swapping | 20 |
| D.3. Combined Text-guided and Style Editing | 21 |
| E Additional Experimental Results | 21 |
| E.1. Text-guided Editing | 21 |
| E.2. Face Swapping | 21 |
| E.3. Combined Text-guided and Style Editing | 22 |
| E.4. Results when Combining with MasaCtrl and Plug-and-Play | 24 |
| F. Ablation Studies | 26 |
| F.1. Impact of \hat{w}^{orig} | 26 |
| F.2. Impact of w^{edit} | 27 |
| F.3. Impact of multiple optimization steps in implicit h -Edit | 27 |
| F.4. Comparison between explicit and implicit versions | 27 |
| F.5. Face swapping without masks | 27 |
| F.6. Running time | 28 |
| G Analysis on Metrics | 28 |
| H Ethical Considerations | 29 |

A. Theoretical Results

A.1. Derivation of the formula of $h(x_t, t)$

Below, we prove that $h(x_t, t)$ satisfying Eqs. 10, 11 can be expressed as follows:

$$h(x_t, t) = \mathbb{E}_{p(x_0|x_t)} [h(x_0, 0)] \quad (31)$$

$$= \mathbb{E}_{p(x_0|x_t)} [p_Y(x_0)] \quad (32)$$

where $p(x_0|x_t)$ is the transition distribution of the base backward Markov process.

We can quickly verify that Eq. 31 is correct for $t = 1$ since $h(x_1, 1) = \int p(x_0|x_1) h(x_0, 0) dx_0 = \mathbb{E}_{p(x_0|x_1)} [h(x_0, 0)]$ directly from Eqs. 10, 11. Assuming that Eq. 31 has been correct for $t - 1$ ($t \geq 2$), we will prove that it is correct for t . The RHS of Eq. 10 can be transformed as follows:

$$h(x_t, t) = \int p(x_{t-1}|x_t) h(x_{t-1}, t-1) dx_{t-1} \quad (33)$$

$$= \int p(x_{t-1}|x_t) \mathbb{E}_{p(x_0|x_{t-1})} [h(x_0, 0)] dx_{t-1} \quad (34)$$

$$= \int p(x_{t-1}|x_t) \left(\int p(x_0|x_{t-1}) h(x_0, 0) dx_0 \right) dx_{t-1} \quad (35)$$

$$= \int \left(\int p(x_0|x_{t-1}) p(x_{t-1}|x_t) dx_{t-1} \right) h(x_0, 0) dx_0 \quad (36)$$

$$= \int p(x_0|x_t) p_Y(x_0) dx_0 \quad (37)$$

$$= \mathbb{E}_{p(x_0|x_t)} [h(x_0, 0)] \quad (38)$$

In Eq. 37, $p(x_0|x_t)$ equals $\int p(x_0|x_{t-1}) p(x_{t-1}|x_t) dx_{t-1}$ because this is the Chapman-Kolmogorov equation [30, 32] for the base backward process. Eq. 38 completes our proof.

A.2. Proof of Proposition 1

First, it can be seen that $p^h(x_{t-1}|x_t)$ is well normalized since according to Eqs. 9, 10, we have:

$$\int p^h(x_{t-1}|x_t) dx_{t-1} = \frac{\int p(x_{t-1}|x_t) h(x_{t-1}, t-1) dx_{t-1}}{h(x_t, t)} \quad (39)$$

$$= \frac{h(x_t, t)}{h(x_t, t)} \quad (40)$$

$$= 1 \quad (41)$$

Thus, $p^h(x_{t-1}|x_t)$ can be viewed as the transition distribution of our bridge. Besides, since x_{t-1} in $p^h(x_{t-1}|x_t)$ only depends on x_t , this bridge is a reverse-time Markov process.

Next, we prove that $p^h(x_t) = \frac{p(x_t)h(x_t, t)}{\mathbb{E}_{p(x_0)}[h(x_0, 0)]}$ for all $t \in [0, T]$. This equation holds for $t = T$ due to our assumption $p^h(x_T) = \frac{p(x_T)h(x_T, T)}{\mathbb{E}_{p(x_0)}[h(x_0, 0)]}$. Assuming that this equation holds for time t , we will prove that it holds for time $t - 1$. Since the bridge is a reverse-time Markov process, we can compute $p^h(x_{t-1})$ as follows:

$$p^h(x_{t-1}) = \int p^h(x_{t-1}|x_t) p^h(x_t) dx_t \quad (42)$$

$$= \int p(x_{t-1}|x_t) \frac{h(x_{t-1}, t-1)}{h(x_t, t)} \frac{p(x_t)h(x_t, t)}{\mathbb{E}_{p(x_0)}[h(x_0, 0)]} dx_t \quad (43)$$

$$= \frac{h(x_{t-1}, t-1) \int p(x_{t-1}|x_t) p(x_t) dx_t}{\mathbb{E}_{p(x_0)}[h(x_0, 0)]} \quad (44)$$

$$= \frac{p(x_{t-1}) h(x_{t-1}, t-1)}{\mathbb{E}_{p(x_0)}[h(x_0, 0)]} \quad (45)$$

where Eq. 43 leverages Eq. 9 and the inductive assumption. Eq. 45 completes our proof.

Finally, we prove that $p^h(x_t)$ is a well normalized distribution as follows:

$$\int p^h(x_t) dx_t = \frac{\int p(x_t) h(x_t, t) dx_t}{\mathbb{E}_{p(x_0)} [h(x_0, 0)]} \quad (46)$$

$$= \frac{\int p(x_t) \mathbb{E}_{p(x_0|x_t)} [h(x_0, 0)] dx_t}{\mathbb{E}_{p(x_0)} [h(x_0, 0)]} \quad (47)$$

$$= \frac{\int p(x_t) (\int p(x_0|x_t) h(x_0, 0) dx_0) dx_t}{\mathbb{E}_{p(x_0)} [h(x_0, 0)]} \quad (48)$$

$$= \frac{\int (\int p(x_t) p(x_0|x_t) dx_t) h(x_0, 0) dx_0}{\mathbb{E}_{p(x_0)} [h(x_0, 0)]} \quad (49)$$

$$= \frac{\int p(x_0) h(x_0, 0) dx_0}{\mathbb{E}_{p(x_0)} [h(x_0, 0)]} \quad (50)$$

$$= 1 \quad (51)$$

The fact that $h(x_t, t) = \mathbb{E}_{p(x_0|x_t)} [h(x_0, 0)]$ in Eq. 47 was proven in Section A.1.

A.3. Closed-form expressions for the explicit and implicit h -Edit updates for Stable Diffusion

In this section, we derive closed-form expressions for the explicit and implicit h -Edit updates corresponding to Eq. 15 and Eq. 18, respectively, for Stable Diffusion (SD). First, we can express $\nabla_{x_t} \log h(x_t, t)$ as follows:

$$\nabla_{x_t} \log h(x_t, t) = \nabla_{x_t} \log p^h(x_t) - \nabla_{x_t} \log p(x_t) \quad (52)$$

$$= \frac{-\tilde{\epsilon}_\theta(x_t, t, c^{\text{edit}})}{\sigma_t} - \frac{-\tilde{\epsilon}_\theta(x_t, t, c^{\text{orig}})}{\sigma_t} \quad (53)$$

$$= \frac{-1}{\sigma_t} (\tilde{\epsilon}_\theta(x_t, t, c^{\text{edit}}) - \tilde{\epsilon}_\theta(x_t, t, c^{\text{orig}})) \quad (54)$$

$$= \frac{-1}{\sigma_t} \left(w^{\text{edit}} \epsilon_\theta(x_t, t, c^{\text{edit}}) + (1 - w^{\text{edit}}) \epsilon_\theta(x_t, t, \emptyset) - (w^{\text{orig}} \epsilon_\theta(x_t, t, c^{\text{orig}}) + (1 - w^{\text{orig}}) \epsilon_\theta(x_t, t, \emptyset)) \right) \quad (55)$$

$$= \frac{-1}{\sigma_t} \left(w^{\text{edit}} \epsilon_\theta(x_t, t, c^{\text{edit}}) - w^{\text{orig}} \epsilon_\theta(x_t, t, c^{\text{orig}}) + (w^{\text{orig}} - w^{\text{edit}}) \epsilon_\theta(x_t, t, \emptyset) \right) \quad (56)$$

$$= \frac{-1}{\sigma_t} f(x_t, t) \quad (57)$$

Finding the formula of η in Eq. 15 can be somewhat tricky. The key is to examine the equation $x_{t-1}^{\text{base}} = x_t + \eta \nabla_{x_t} \log p(x_t) + \sqrt{2\eta}z$ in Eq. 14, which can be interpreted as sampling x_{t-1}^{base} from the Gaussian backward transition distribution $p_\theta(x_{t-1}|x_t)$. This implies that if we omit the random term $\sqrt{2\eta}z$, the simplified equation $x_{t-1}^{\text{base}} = x_t + \eta \nabla_{x_t} \log p(x_t)$ corresponds to the mean of $p_\theta(x_{t-1}|x_t)$, as provided in Eq. 4, and rewritten as follows:

$$x_{t-1}^{\text{base}} = \frac{a_{t-1}}{a_t} x_t + \underbrace{\left(\sqrt{\sigma_{t-1}^2 - \omega_{t,t-1}^2} - \frac{\sigma_t a_{t-1}}{a_t} \right)}_{\tilde{\mu}_{\theta, \omega, t, t-1}(x_t, c^{\text{orig}})} \tilde{\epsilon}_\theta(x_t, t, c^{\text{orig}}) \quad (58)$$

$$= \frac{a_{t-1}}{a_t} x_t + \left(\sqrt{\sigma_{t-1}^2 - \omega_{t,t-1}^2} - \frac{\sigma_t a_{t-1}}{a_t} \right) (w^{\text{orig}} \epsilon_\theta(x_t, t, c^{\text{orig}}) + (1 - w^{\text{orig}}) \epsilon_\theta(x_t, t, \emptyset)) \quad (59)$$

$$= \frac{a_{t-1}}{a_t} x_t - \left(\sqrt{\sigma_{t-1}^2 - \omega_{t,t-1}^2} - \frac{\sigma_t a_{t-1}}{a_t} \right) \sigma_t \nabla_{x_t} \log p(x_t) \quad (60)$$

Eq. 60 suggests that $\eta = - \left(\sqrt{\sigma_{t-1}^2 - \omega_{t,t-1}^2} - \frac{\sigma_t a_{t-1}}{a_t} \right) \sigma_t$. One can easily verify that $\eta > 0$. It is worth noting that there is a little mismatch between the coefficients of x_t in Eq. 58 and in $x_{t-1}^{\text{base}} = x_t + \eta \nabla_{x_t} \log p(x_t)$. This is expected because the

standard LMC update assumes a forward diffusion process governed by the SDE $dx_t = \sqrt{2}dw_t$, which lacks a drift term. In contrast, the continuous-time forward process of Stable Diffusion follows the SDE $dx_t = \frac{-\beta_t}{2}x_t dt + \sqrt{\beta_t}dw_t$, which has the drift term $\frac{-\beta_t}{2}x_t$.

It can be inferred that u_t^{orig} mimics the random term $\sqrt{2\eta}z$, with the key difference being that it is precomputed during the forward pass rather than randomly sampled during the backward pass.

According to the above analysis, the explicit h -Edit update for Stable Diffusion is given by:

$$x_{t-1}^{\text{base}} = \underbrace{\tilde{\mu}_{\theta, \omega, t, t-1}(x_t^{\text{edit}}, c^{\text{orig}})}_{x_t + \eta \nabla \log p(x_t)} + \underbrace{u_t^{\text{orig}}}_{\sqrt{2\eta}z} \quad (61)$$

$$x_{t-1}^{\text{edit}} = x_{t-1}^{\text{base}} + \underbrace{\left(- \left(\sqrt{\sigma_{t-1}^2 - \omega_{t,t-1}^2} - \frac{\sigma_t a_{t-1}}{a_t} \right) \sigma_t \right)}_{\eta} \underbrace{\frac{-1}{\sigma_t} f(x_t^{\text{edit}}, t)}_{\nabla \log h(x_t, t)} \quad (62)$$

$$= x_{t-1}^{\text{base}} + \left(\sqrt{\sigma_{t-1}^2 - \omega_{t,t-1}^2} - \frac{\sigma_t a_{t-1}}{a_t} \right) f(x_t^{\text{edit}}, t) \quad (63)$$

To derive the implicit h -Edit update, we first write Eq. 58 in the implicit form $x_{t-1} = \frac{a_{t-1}}{a_t}x_t + \left(\sqrt{\sigma_{t-1}^2 - \omega_{t,t-1}^2} - \frac{\sigma_t a_{t-1}}{a_t} \right) \tilde{\epsilon}_{\theta}(x_{t-1}, t-1, c^{\text{orig}})$, which reveals that $\gamma = - \left(\sqrt{\sigma_{t-1}^2 - \omega_{t,t-1}^2} - \frac{\sigma_t a_{t-1}}{a_t} \right) \sigma_{t-1}$. Using this, we compute x_{t-1}^{edit} based on the formula in Eq. 18 as follows:

$$x_{t-1}^{\text{edit}} = x_{t-1}^{\text{base}} + \gamma \nabla_{x_{t-1}} h(x_{t-1}^{\text{base}}, t-1) \quad (64)$$

$$= x_{t-1}^{\text{base}} + \left(- \left(\sqrt{\sigma_{t-1}^2 - \omega_{t,t-1}^2} - \frac{\sigma_t a_{t-1}}{a_t} \right) \sigma_{t-1} \right) \frac{1}{\sigma_{t-1}} f(x_{t-1}^{\text{base}}, t-1) \quad (65)$$

$$= x_{t-1}^{\text{base}} + \left(\sqrt{\sigma_{t-1}^2 - \omega_{t,t-1}^2} - \frac{\sigma_t a_{t-1}}{a_t} \right) f(x_{t-1}^{\text{base}}, t-1) \quad (66)$$

where x_{t-1}^{base} is given in Eq. 61.

One advantage of the natural disentanglement in the h -Edit update is that the guidance scales w^{orig} for computing x_{t-1}^{base} in Eq. 59 and w^{orig} for computing $\nabla \log h(x_t, t)$ in Eq. 56 do *not* need to be the same. This allows w^{orig} in Eq. 59 to follow the guidance scale used in the forward pass, while w^{orig} in Eq. 56 can be chosen arbitrarily. To emphasize this distinction, we denote w^{orig} in Eq. 56 as \hat{w}^{orig} , indicating that it may differ from w^{orig} in Eq. 59. This \hat{w}^{orig} can be interpreted as a hyperparameter controlling how much of the original image’s information is excluded from the editing process. During our experiments, we observed that w^{orig} , \hat{w}^{orig} , and w^{edit} should be chosen such that $0 < w^{\text{orig}} \leq \hat{w}^{\text{orig}} < w^{\text{edit}}$.

B. Algorithms

B.1. h -Edit for Combined Editing

In Algorithms 1 and 2, we provide pseudo-codes for the explicit and implicit versions of h -Edit for combined text-guided and reward-model-based editing.

Algorithm 1 Explicit h -Edit for combined editing, compatible with both deterministic and random inversion, and supporting integration with the P2P [19].

Require: Original image x_0^{orig} , reference image x_0^{ref} , original text c^{orig} , edited text c^{edit} , guidance weights w^{orig} , w^{edit} , \hat{w}^{orig} , external encoder G , external distance loss \mathcal{L} , external guidance weight ρ_t .

- 1: $\left\{x_t^{\text{orig}}\right\}_{t=1}^T, \left\{u_t^{\text{orig}}\right\}_{t=1}^T = \text{Inversion}\left(x_0^{\text{orig}}, c^{\text{orig}}\right)$
- 2: $x_T^{\text{edit}} = x_T^{\text{orig}}$
- 3: **for** $t = T, \dots, 1$ **do**
- 4: $x_t = x_t^{\text{edit}}$
- 5: $\tilde{\epsilon}_\theta(x_t, t, c^{\text{orig}}) = w^{\text{orig}}\epsilon_\theta(x_t, t, c^{\text{orig}}) + (1 - w^{\text{orig}})\epsilon_\theta(x_t, t, \emptyset)$
- 6: Compute $\tilde{\mu}_{\theta, \omega, t, t-1}(x_t, c^{\text{orig}})$ from $\tilde{\epsilon}_\theta(x_t, t, c^{\text{orig}})$ via Eq. 2
- 7: $x_{t-1}^{\text{base}} = \tilde{\mu}_{\theta, \omega, t, t-1}(x_t, c^{\text{orig}}) + u_t^{\text{orig}}$
- 8: **if** text-guided editing **then**
- 9: **if** combined with P2P **then**
- 10: Get the attention map M_t^{edit} from $\epsilon_\theta(x_t, t, c^{\text{edit}})$
- 11: Get the attention map M_t^{orig} from $\epsilon_\theta(x_t^{\text{orig}}, t, c^{\text{orig}})$
- 12: $\hat{M}_t^{\text{edit}} = \text{P2P}\left(M_t^{\text{edit}}, M_t^{\text{orig}}, t\right)$
- 13: Apply the new attention map \hat{M}_t^{edit} to $\epsilon_\theta(x_t, t, c^{\text{edit}})$
- 14: **end if**
- 15: $f(x_t, t) = w^{\text{edit}}\epsilon_\theta(x_t, t, c^{\text{edit}}) - \hat{w}^{\text{orig}}\epsilon_\theta(x_t, t, c^{\text{orig}}) + (\hat{w}^{\text{orig}} - w^{\text{edit}})\epsilon_\theta(x_t, t, \emptyset)$
- 16: $\hat{x}_{t-1} = x_{t-1}^{\text{base}} + \left(\sqrt{\sigma_{t-1}^2 - \omega_{t,t-1}^2 - \frac{\sigma_t a_{t-1}}{a_t}}\right) f(x_t, t)$
- 17: $\hat{\epsilon}_t = \text{stop_grad}\left(w^{\text{edit}}\epsilon_\theta(x_t, t, c^{\text{edit}}) + (1 - w^{\text{edit}})\epsilon_\theta(x_t, t, \emptyset)\right)$
- 18: **else**
- 19: $\hat{x}_{t-1} = x_{t-1}^{\text{base}}$
- 20: $\hat{\epsilon}_t = \text{stop_grad}\left(w^{\text{orig}}\epsilon_\theta(x_t, t, c^{\text{orig}}) + (1 - w^{\text{orig}})\epsilon_\theta(x_t, t, \emptyset)\right)$
- 21: **end if**
- 22: $x_{0|t} = \frac{x_t - \sigma_t \hat{\epsilon}_t}{a_t}$
- 23: $g_t = -\nabla_{x_t} \mathcal{L}\left(G(x_{0|t}), G(x_0^{\text{ref}})\right)$
- 24: $x_{t-1}^{\text{edit}} = \hat{x}_{t-1} + \rho_t g_t$
- 25: **if** text-guided editing **and** combined with P2P **and** local blending **then**
- 26: $x_{t-1}^{\text{edit}} = \text{local_blend}\left(x_{t-1}^{\text{edit}}, x_{t-1}^{\text{orig}}\right)$
- 27: **end if**
- 28: **end for**

Algorithm 2 Implicit h -Edit for combined editing, compatible with both deterministic and random inversions, and supporting integration with the P2P [19].

Require: Original image x_0^{orig} , reference image x_0^{ref} , original text c^{orig} , edited text c^{edit} , guidance weights w^{orig} , w^{edit} , \hat{w}^{orig} , reconstruction weight λ_t , external encoder G , external distance loss \mathcal{L} , external guidance weight ρ_t , number of implicit loops K .

- 1: $\left\{x_t^{\text{orig}}\right\}_{t=1}^T, \left\{u_t^{\text{orig}}\right\}_{t=1}^T = \text{Inversion} \left(x_0^{\text{orig}}, c^{\text{orig}}\right)$
- 2: $x_T^{\text{edit}} = x_T^{\text{orig}}$
- 3: **for** $t = T, \dots, 1$ **do**
- 4: $x_t = x_t^{\text{edit}}$
- 5: $\tilde{\epsilon}_\theta \left(x_t, t, c^{\text{orig}}\right) = w^{\text{orig}} \epsilon_\theta \left(x_t, t, c^{\text{orig}}\right) + \left(1 - w^{\text{orig}}\right) \epsilon_\theta \left(x_t, t, \emptyset\right)$
- 6: **Compute** $\tilde{\mu}_{\theta, \omega, t, t-1} \left(x_t, c^{\text{orig}}\right)$ from $\tilde{\epsilon}_\theta \left(x_t, t, c^{\text{orig}}\right)$ via Eq. 2
- 7: $x_{t-1}^{\text{base}} = \tilde{\mu}_{\theta, \omega, t, t-1} \left(x_t, c^{\text{orig}}\right) + u_t^{\text{orig}}$
- 8: $x_{t-1}^{(0)} = x_{t-1}^{\text{base}}$
- 9: **for** $k = 0, \dots, K - 1$ **do**
- 10: **if** improving reconstruction **then**
- 11: $r_{t-1} = x_{t-1}^{(k)} - x_{t-1}^{\text{base}}$
- 12: $x_{t-1}^{(k)} = x_{t-1}^{(k)} - \lambda_{t-1} r_{t-1}$
- 13: **end if**
- 14: **if** text-guided editing **then**
- 15: **if** combined with P2P **then**
- 16: Get the attention map M_{t-1}^{edit} from $\epsilon_\theta \left(x_{t-1}^{(k)}, t - 1, c^{\text{edit}}\right)$
- 17: Get the attention map M_{t-1}^{orig} from $\epsilon_\theta \left(x_{t-1}^{\text{orig}}, t - 1, c^{\text{orig}}\right)$
- 18: $\hat{M}_{t-1}^{\text{edit}} = \text{P2P} \left(M_{t-1}^{\text{edit}}, M_{t-1}^{\text{orig}}, t - 1\right)$
- 19: Apply the new attention map $\hat{M}_{t-1}^{\text{edit}}$ to $\epsilon_\theta \left(x_{t-1}^{(k)}, t - 1, c^{\text{edit}}\right)$
- 20: **end if**
- 21: $f \left(x_{t-1}^{(k)}, t - 1\right) = w^{\text{edit}} \epsilon_\theta \left(x_{t-1}^{(k)}, t - 1, c^{\text{edit}}\right) - \hat{w}^{\text{orig}} \epsilon_\theta \left(x_{t-1}^{(k)}, t - 1, c^{\text{orig}}\right) + \left(\hat{w}^{\text{orig}} - w^{\text{edit}}\right) \epsilon_\theta \left(x_{t-1}^{(k)}, t - 1, \emptyset\right)$
- 22: $\hat{x}_{t-1} = x_{t-1}^{(k)} + \left(\sqrt{\sigma_{t-1}^2 - \omega_{t,t-1}^2 - \frac{\sigma_{t,a_{t-1}}}{a_t}}\right) f \left(x_{t-1}^{(k)}, t - 1\right)$
- 23: $\hat{\epsilon}_{t-1} = \text{stop_grad} \left(w^{\text{edit}} \epsilon_\theta \left(x_{t-1}^{(k)}, t - 1, c^{\text{edit}}\right) + \left(1 - w^{\text{edit}}\right) \epsilon_\theta \left(x_{t-1}^{(k)}, t - 1, \emptyset\right)\right)$
- 24: **else**
- 25: $\hat{x}_{t-1} = x_{t-1}^{(k)}$
- 26: $\hat{\epsilon}_{t-1} = \text{stop_grad} \left(w^{\text{orig}} \epsilon_\theta \left(x_{t-1}^{(k)}, t - 1, c^{\text{orig}}\right) + \left(1 - w^{\text{orig}}\right) \epsilon_\theta \left(x_{t-1}^{(k)}, t - 1, \emptyset\right)\right)$
- 27: **end if**
- 28: $x_{0|t-1} = \frac{\hat{x}_{t-1} - \sigma_{t-1} \hat{\epsilon}_{t-1}}{a_{t-1}}$
- 29: $g_{t-1} = -\nabla_{\hat{x}_{t-1}} \mathcal{L} \left(G \left(x_{0|t-1}\right), G \left(x_0^{\text{ref}}\right)\right)$
- 30: $x_{t-1}^{(k+1)} = \hat{x}_{t-1} + \rho_{t-1} g_{t-1}$
- 31: **end for**
- 32: $x_{t-1}^{\text{edit}} = x_{t-1}^{(K)}$
- 33: **if** text-guided editing **and** combined with P2P **and** local blending **then**
- 34: $x_{t-1}^{\text{edit}} = \text{local_blend} \left(x_{t-1}^{\text{edit}}, x_{t-1}^{\text{orig}}\right)$
- 35: **end if**
- 36: **end for**

B.2. Edit Friendly for Combined Editing

In this work, we extend Edit Friendly [24] to combined text-guided and reward-model-based editing tasks by combining it with the technique in [79]. The pseudo-code for this extension is provided in Algorithm 3. This extension serves as a baseline for our method in the combined editing setting.

Algorithm 3 Edit Friendly for combined editing, supporting integration with the P2P [19].

Require: Original image x_0^{orig} , reference image x_0^{ref} , original text c^{orig} , edited text c^{edit} , guidance weights w^{orig} , w^{edit} , external encoder G , external distance loss \mathcal{L} , external guidance weight ρ_t .

```

1:  $x_T^{\text{orig}}, \{u_t^{\text{orig}}\}_{t=1}^T = \text{RandomInversion}(x_0^{\text{orig}}, c^{\text{orig}})$ 
2:  $x_T^{\text{edit}} = x_T^{\text{orig}}$ 
3: for  $t = T, \dots, 1$  do
4:    $x_t = x_t^{\text{edit}}$ 
5:   if text-guided editing then
6:     if combined with P2P then
7:       Get the attention map  $M_t^{\text{edit}}$  from  $\epsilon_\theta(x_t, t, c^{\text{edit}})$ 
8:       Get the attention map  $M_t^{\text{orig}}$  from  $\epsilon_\theta(x_t^{\text{orig}}, t, c^{\text{orig}})$ 
9:        $\hat{M}_t^{\text{edit}} = \text{P2P}(M_t^{\text{edit}}, M_t^{\text{orig}}, t)$ 
10:      Apply the new attention map  $\hat{M}_t^{\text{edit}}$  to  $\epsilon_\theta(x_t, t, c^{\text{edit}})$ 
11:    end if
12:     $\tilde{\epsilon}_\theta(x_t, t) = w^{\text{edit}}\epsilon_\theta(x_t, t, c^{\text{edit}}) + (1 - w^{\text{edit}})\epsilon_\theta(x_t, t, \emptyset)$ 
13:  else
14:     $\tilde{\epsilon}_\theta(x_t, t) = w^{\text{orig}}\epsilon_\theta(x_t, t, c^{\text{orig}}) + (1 - w^{\text{orig}})\epsilon_\theta(x_t, t, \emptyset)$ 
15:  end if
16:  Compute  $\tilde{\mu}_{\theta, \omega, t, t-1}(x_t, t)$  from  $\tilde{\epsilon}_\theta(x_t, t)$  via Eq. 2
17:   $x_{0|t} = \frac{x_t - \sigma_t \tilde{\epsilon}_\theta(x_t, t)}{a_t}$  where  $a_t = \sqrt{\bar{\alpha}_t}$  and  $\sigma_t = \sqrt{1 - \bar{\alpha}_t}$ 
18:   $g_t = -\nabla_{x_t} \mathcal{L}(G(x_{0|t}), G(x_0^{\text{ref}}))$ 
19:   $x_{t-1}^{\text{edit}} = \tilde{\mu}_{\theta, \omega, t, t-1}(x_t, t) + \rho_t g_t + u_t^{\text{orig}}$ 
20:  if text-guided editing and combined with P2P and local blending then
21:     $x_{t-1}^{\text{edit}} = \text{local\_blend}(x_{t-1}^{\text{edit}}, x_{t-1}^{\text{orig}})$ 
22:  end if
23: end for
24: return  $x_0^{\text{edit}}$ 

```

C. Additional Discussion on Related Work

C.1. Training-based Editing

Training-based approaches, such as DiffusionCLIP [33] and Asyrp [35], modify the noise network of a pretrained diffusion model through fine-tuning or by incorporating an auxiliary network, resulting in a new noise network that supports generating images with the desired editing attributes. The local directional CLIP loss [17] is commonly used as the training objective. However, these methods require training a new network for each specific editing target, limiting their adaptability to diverse editing scenarios in practice. In contrast, InstructPix2Pix [4] trains an entirely new diffusion model that generates images based on editing instructions. The instruction texts and target edited images for training are generated by GPT-3 [5] and P2P [19], respectively, meaning that the quality of the edits is inherently tied to P2P’s performance. Additionally, the high training cost remains a significant drawback of this method.

C.2. Conditional Generation with Diffusion Models

The goal of conditional generation is to sample data from the joint distribution $p(x_0)p(y|x_0)$, which can be achieved by learning the score $\nabla \log p(x_t, y)$ of the joint distribution $p(x_t, y)$ via the score matching framework [25, 65]. Class-guided diffusion model [12] learns a noisy classifier $p(y|x_t)$ and combines its gradient with the score $\nabla \log p(x_t)$ learned by another unconditional diffusion model (e.g., DDPM [22]) to obtain $\nabla \log p(x_t, y)$. Meanwhile, classifier-free guidance [21] simultaneously learn both $\nabla \log p(x_t)$ and $\nabla \log p(x_t|y)$ using a single noise network. Energy-guided SDE (EGSDE) [83] extends class-guided diffusion models to solve the image-to-image translation problem. It utilizes a noisy classifier pretrained on both the source and target domains to define a similarity score between noisy samples from the two domains. This score acts as a negative energy guiding the generation of target domain samples toward preserving some properties of the corresponding source domain samples. The energy-based perspective have also been considered in works on generating compositional concepts with diffusion models [40]. FreeDom [79] approximates the time-dependent energy function in EGSDE using Tweedie’s formula: $\mathcal{E}(c, x_t, t) = \mathbb{E}_{p(x_0|x_t)}[\mathcal{E}(c, x_0, t)] \approx \mathcal{E}(c, x_0|t, t)$ [9, 16]. This eliminates the reliance on a noisy classifier which is often difficult to obtain in practice and allows FreeDom to leverage any available pretrained model on clean samples x_0 to define the energy function. As a result, FreeDom supports conditional information from segmentation maps, style images, and face IDs. Similarly, UGD [2] utilizes Tweedie’s formula but employs a different reparameterization for guidance using external networks.

The EGSDE framework can be considered as a special case of our reverse-time bridge modeling framework, as ours applies to more general Markov processes rather than just diffusion SDEs. Our framework also provides a formula for the bridge’s transition distribution, enabling ancestral sampling in a discrete-time setting. Meanwhile, EGSDE usually relies on the Euler-Maruyama method for approximate sampling because it only has access to the instantaneous velocity at time t .

C.3. Diffusion Bridges and Doob’s h -Transform

Most diffusion bridge methods [10, 39, 41, 63, 85] focus on the image-to-image translation problem which involves matching two explicit distributions of two domains A, B. They typically assume a diffusion model that generates domain A from Gaussian noise is given, and apply Doob’s h -transform [15] to the forward process of this diffusion model to map samples of domain A to those of domain B rather than Gaussian noise. Some approaches like [41, 63] directly learn the h -function, while others [85] utilize an analytical form of the h -function and learn the score of the reverse bridge. Our method, in contrast, applies Doob’s h -transform to the backward process to map Gaussian noise to samples with the desired target attributes.

D. Further Details on Experimental Settings

D.1. Text-guided Editing

The P2P hyperparameters for deterministic-inversion-based methods with P2P (including h -Edit-D + P2P) were configured based on the setup in [27]. Specifically, the sampling step proportions for self-attention and cross-attention controls were set to 0.6 and 0.4, respectively. For h -Edit-R and EF with P2P, the proportion of sampling steps for self-attention control was adjusted to 0.35, as 0.6 was found to be excessive for effective editing with these methods. For h -Edit-R and EF without P2P, the first 15 steps were skipped to ensure faithful reconstruction, as recommended in [24]. This skipping was not required for their P2P counterparts. For LEDITS++ [3], we adhered to the hyperparameters specified in the original paper.

D.2. Face Swapping

We utilized the official pretrained models for MegaFS, AFS, and DiffFace, available at [MegaFS](#), [AFS](#), and [DiffFace](#), respectively. Since the official pretrained model for FaceShifter is unavailable, we used an unofficial pretrained model from [this repository](#). For evaluation, we employed a pretrained ArcFace model with the IR-SE-50 backbone ([68, 79]), available through the [InsightFace](#) library for evaluation. This model was also used in h -Edit-R, EF, and FaceShifter¹ for generating swapped faces. For DiffFace, the ArcFace model with the ResNet101 backbone from its official code was used for face swapping. MegaFS and AFS relied on the ArcFace model with the IR-SE-50 backbone during training but not during face swapping. Additional evaluations using other face identity representation models are provided in Appendix E.2. CelebA-HQ images were resized to 256×256 and cropped as $x=x[: , : , 35:223, 32:220]$ to prepare them for input into the ArcFace model. Following [79], we defined the coefficient ρ_t for the identity similarity reward gradient (Algorithms 2, 1, 3) as $\rho^{\text{face}} \times \sqrt{\bar{\alpha}_t}$, where $\bar{\alpha}_t$ is the Stable Diffusion scheduler coefficient at time step t . For h -Edit-R and EF, ρ^{face} was set to 100.0. For h -Edit-R (3s), ρ^{face} was reduced to 50.0, which provided a better balance between editing effectiveness and

¹FaceShifter uses the ArcFace model with the IR-SE-50 backbone to extract face identity embeddings during both training and generating swapped faces.

faithfulness when using three optimization steps. To further enhance faithfulness to the original image, we incorporated the negative LPIPS score as an additional reward alongside identity similarity. The LPIPS score, computed using a pretrained VGG network, measures the perceptual similarity between x_0^{edit} and x_0^{orig} . The coefficient for this reward is similar to that of the identity similarity reward. For post-processing, we applied a mask generated by the face parsing model in [78] to preserve the original background while applying edits to the face. This procedure was consistent across all baselines. The face swapping results without using masks are provided in Appdx. F.5.

D.3. Combined Text-guided and Style Editing

In combined text-guided and style editing, we disabled local blending in P2P as our experiments indicated that it negatively impacts style editing performance. For EF + P2P, following [79], we scaled the gradient norm of the style loss reward at each time t by the norm of $[\epsilon(x_t, t, c^{\text{edit}}) - \epsilon(x_t, t, \emptyset)]$. This corresponds to defining the coefficient ρ_t for style editing in EF + P2P as:

$$\rho_t := \rho^{\text{sty}} * \frac{\|(\epsilon(x_t, t, c^{\text{edit}}) - \epsilon(x_t, t, \emptyset))\|_2}{\|g_t\|_2} \tag{67}$$

For h -Edit-R + P2P, we scaled the gradient norm of the style reward to match the norm of the text-guided editing function $f(\cdot)$ in Eq. 24. This approach leverages the disentangled update mechanism unique to our method (Sections 3 and A.3). Accordingly, the coefficient ρ_t for the style editing term in h -Edit-R + P2P is defined as:

$$\rho_t := \rho^{\text{sty}} * \frac{\|f(x_t, t)\|_2}{\|g_t\|_2} \tag{68}$$

E. Additional Experimental Results

E.1. Text-guided Editing

E.1.1 Deterministic-inversion-based methods

Fig. 5 shows additional edited images produced by h -Edit-D + P2P alongside other deterministic-inversion-based editing methods with P2P [7, 27, 38, 45, 46]. h -Edit-D + P2P consistently outperforms the baselines in handling difficult edits, while maintaining faithful reconstruction, as reflected in the quantitative results in Table 1. For instance, our method successfully removes the boy’s tie (first row, right) and transforms the car into a motorcycle (seventh row, right), tasks where most other methods struggle. Although NP + P2P and NT + P2P demonstrate strong editing capabilities, as evidenced by their high local CLIP similarity scores in Table 1, they are not good at preserving non-edited content compared to other methods. Conversely, NMG + P2P, StyleD + P2P, and PnP Inv + P2P achieve high fidelity to the original image, but fail to deliver effective edits in many cases.

E.1.2 Random-inversion-based methods

In Fig. 6, we present additional visual comparisons of h -Edit-R + P2P against EF + P2P and LEDITS++. These visualizations are consistent with the quantitative results in Table 1, confirming that our method surpasses both EF + P2P and LEDITS++ in editing effectiveness and faithfulness. Further qualitative results of h -Edit-R and EF without P2P are shown in Fig. 7, where our method once again demonstrates superior performance.

E.2. Face Swapping

Since h -Edit-R, EF, and FaceShifter utilize the same ArcFace model for both face swapping and evaluation, this may lead to more favorable identity matching results for these methods compared to other baselines. To ensure a fair comparison, we reassessed the identity transfer quality of all methods using alternative face identity representation models. Specifically, we used VGG-Face [49], FaceNet128, FaceNet512 [59] and ArcFace with the ResNet34 backbone. These models were implemented in TensorFlow with pretrained weights available through the DeepFace repository [60, 61]. Quantitative results of this evaluation are provided in Table 2.

Interestingly, DiffFace achieves the best performance across all face identity representation models used for evaluation. h -Edit-R (3s) and h -Edit-R rank second and third, respectively, outperforming EF and FaceShifter but falling slightly short of DiffFace. This demonstrates that our method is capable of effective face swapping, even without being explicitly trained for this task like DiffFace, as further illustrated by the qualitative results in Fig. 8. We hypothesize that DiffFace’s good

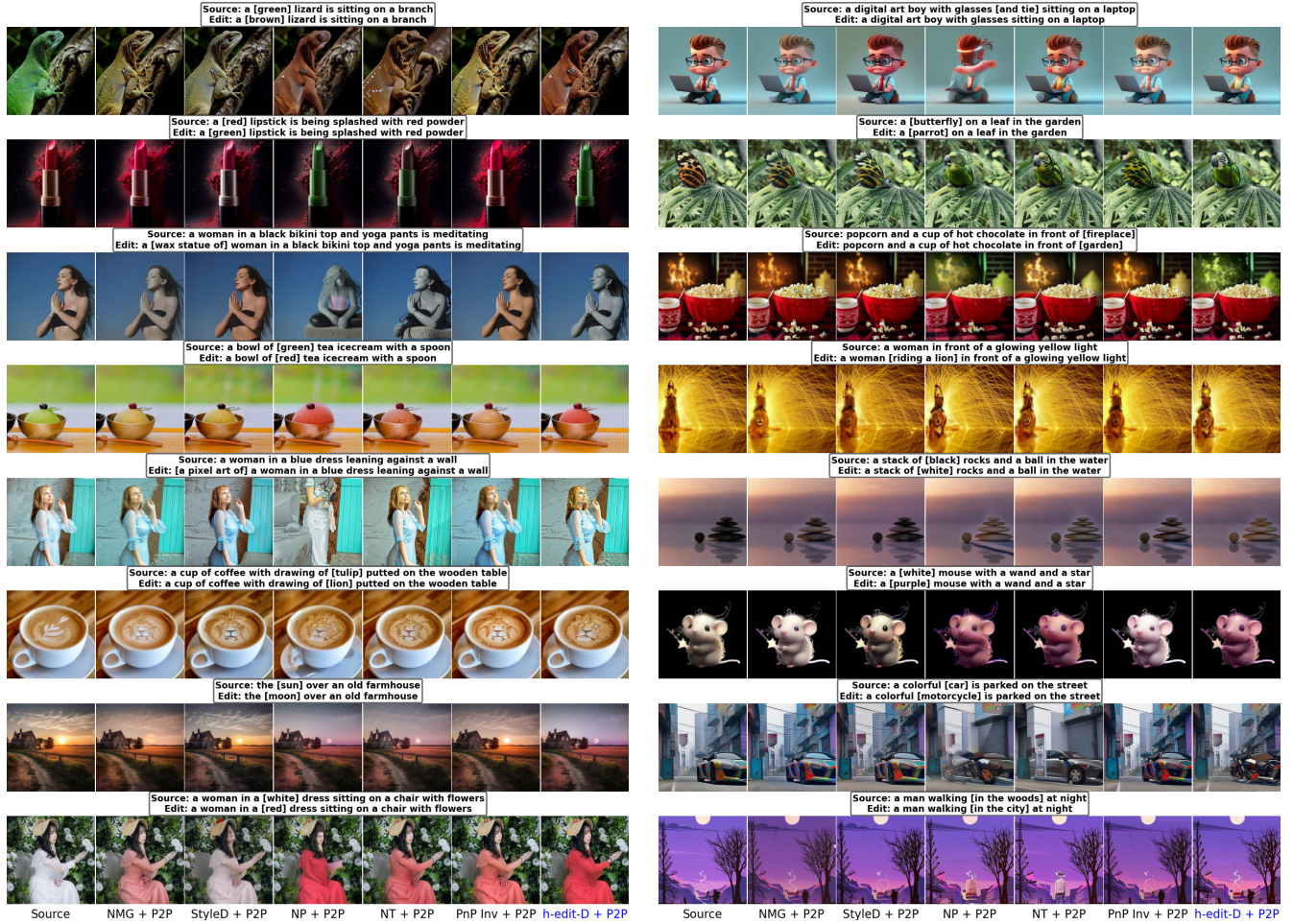


Figure 5. Additional visual comparisons between h -Edit-D + P2P and other deterministic-inversion-based methods with P2P.

| Model | Metric | FaceShifter | MegaFS | AFS | DiffFace | EF | h -edit-R | h -edit-R (3s) |
|--------------------|------------------------|-------------|--------|------|-------------|------|-------------|------------------|
| ArcFace (ResNet34) | Cosine Sim. \uparrow | 0.54 | 0.33 | 0.44 | 0.56 | 0.50 | 0.52 | <u>0.55</u> |
| VGG-Face | L2 Dist. \downarrow | 0.99 | 1.12 | 1.03 | 0.96 | 1.02 | 1.00 | <u>0.97</u> |
| FaceNet128 | L2 Dist. \downarrow | 0.83 | 1.02 | 0.86 | 0.77 | 0.83 | <u>0.80</u> | 0.77 |
| FaceNet512 | L2 Dist. \downarrow | <u>0.81</u> | 1.01 | 0.87 | 0.77 | 0.83 | <u>0.81</u> | 0.77 |

Table 2. Face identity transfer results evaluated using face identity representation models different from the ArcFace model with the IR-SE-50 backbone.

performance may be attributed to (i) its use of an ArcFace model with a larger backbone (ResNet101) for face swapping and (ii) training on a larger dataset compared to the pretrained diffusion model employed by our method.

E.3. Combined Text-guided and Style Editing

Fig. 9 illustrates the changes in style loss, local CLIP similarity, and LPIPS score as the style editing coefficient ρ^{sty} is varied from 0.1 to 1.0 for h -Edit-R + P2P and from 1.1 to 2.0 for EF + P2P. While the ranges of ρ^{sty} differ, the resulting style loss, local CLIP similarity, and LPIPS score ranges are comparable, validating the appropriateness of our parameter selection. Increasing ρ^{sty} improves style transfer (lower style loss) but compromises text-guided editing quality in terms of both effectiveness and faithfulness (lower local CLIP similarity and higher LPIPS respectively). Since determining the

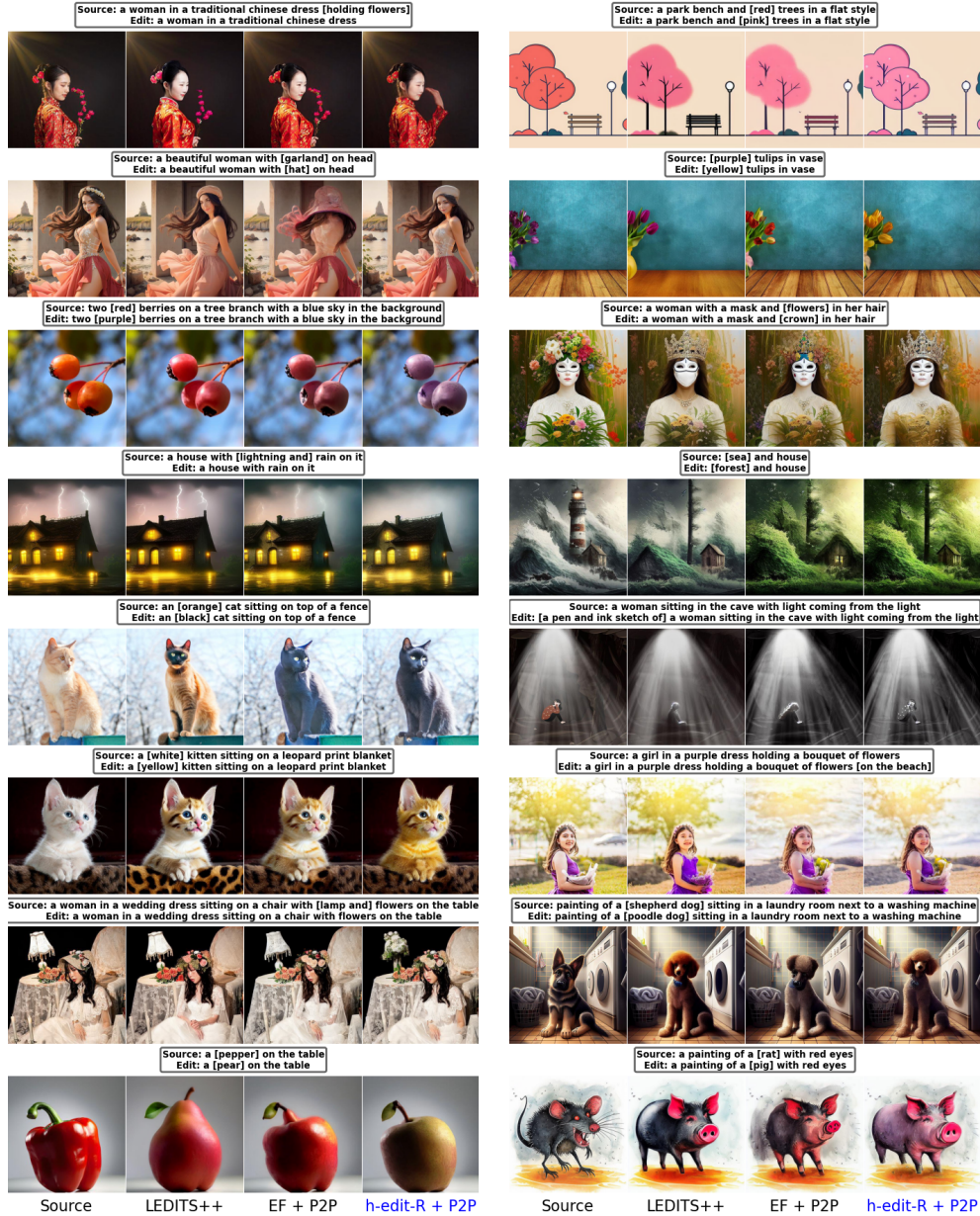


Figure 6. Additional qualitative results of h -Edit-R, EF, and LEDITS+++ with P2P.

optimal value of ρ^{sty} for achieving a balance between style and text-guided editing is nontrivial, we identified candidate values near the intersection of the style loss and LPIPS curves. Combining this with visual inspection, we selected ρ^{sty} value of 0.6 for h -Edit-R and 1.5 for EF.

Although EF exhibits similar quantitative trends to our method when ρ^{sty} is varied, its qualitative behavior is notably different. As shown in Fig. 10, our method smoothly incorporates more style information into the edited images while preserving their global structure as ρ^{sty} increases. In contrast, EF often modifies the global structure of the images to accommodate the increased ρ^{sty} . This advantage of our approach likely stems from the natural decomposition of the update into reconstruction and editing terms (Eq. 18), enabling style edits to be added to the text-guided editing term with minimal impact on the reconstruction term. EF, on the other hand, lacks such a decomposition, meaning the introduction of the style editing term directly affects reconstruction. These findings highlight the limitations of relying solely on quantitative metrics to compare our method with EF, as they may fail to capture important qualitative differences.

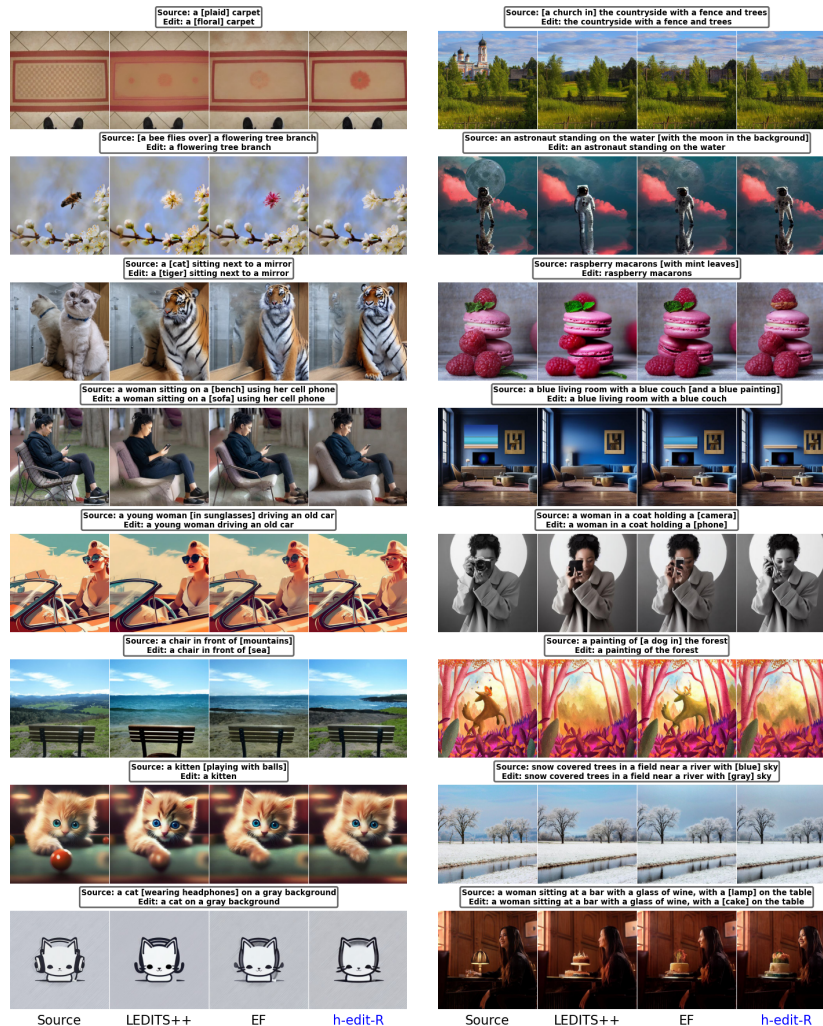


Figure 7. Additional qualitative results of h -Edit-R, EF (without P2P), and LEDITS++.

In Fig. 11, we present additional visualizations comparing h -Edit-R + P2P and EF + P2P, with ρ^{sty} set to the optimal values for each method. The results clearly demonstrate that our method combined with P2P surpasses EF + P2P in both style transfer and text-guided editing, achieving superior quality and consistency.

E.4. Results when Combining with MasaCtrl and Plug-and-Play

In this section, we compare the performance of h -Edit with other baselines when combined with MasaCtrl [6] and Plug-and-Play (PnP) [70]. For MasaCtrl, we adopted the implementation from the PnP Inversion paper [27] which omits the source prompt during editing. We observed that this approach yields more stable results compared to using the source prompt. Since editing methods like NT, NP and NMG are incompatible with this setting, they were excluded in our experiments with MasaCtrl.

As shown in Table 3, both h -Edit-R and h -Edit-D significantly outperform EF and deterministic-inversion-based baselines when combined with either MasaCtrl or PnP. For example, with PnP, h -Edit-D and h -Edit-R surpass NT and EF by 0.014 and 0.029 on the local directional CLIP metric, while achieving about 0.70 and 0.90 lower LPIPS scores, respectively. It is also evident that PnP is a more effective attention control method than MasaCtrl on the PIE-Bench dataset. However, both PnP and MasaCtrl are less effective and stable than P2P [19], as indicated by our quantitative results in Tables 1 and 3, and through our observations.



Figure 8. Additional qualitative comparisons between our method and other face swapping baselines. Identity similarity scores (higher is better) computed using ArcFace with the ResNet34 backbone are displayed below each output.

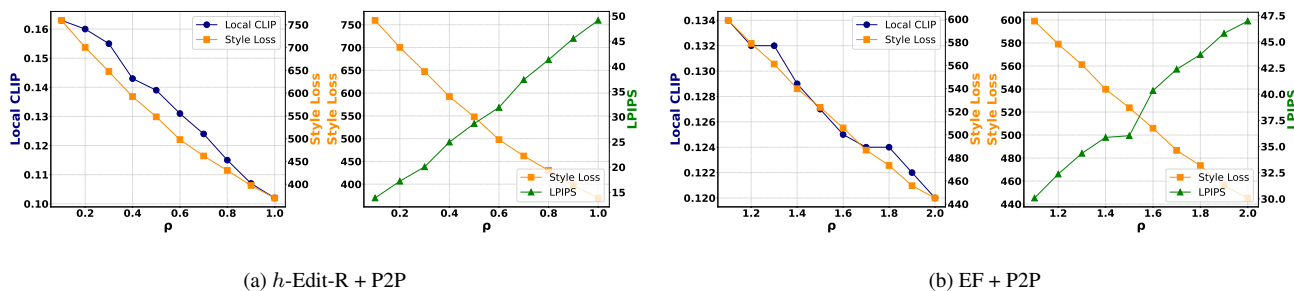


Figure 9. Changes in style loss, local CLIP similarity, and LPIPS score of h -Edit-R + P2P and EF + P2P when ρ^{sty} is varied from 0.1 to 1.0 for h -Edit-R + P2P and from 1.1 to 2.0 for EF + P2P.

| Attn. | Inv. | Method | CLIP Sim. \uparrow | Local CLIP \uparrow | DINO Dist. $\times 10^2\downarrow$ | LPIPS $\times 10^2\downarrow$ | SSIM $\times 10\uparrow$ | PSNR \uparrow |
|----------|--------|-------------|----------------------|-----------------------|------------------------------------|-------------------------------|--------------------------|-----------------|
| MasaCtrl | Deter. | PnP Inv | 0.243 | 0.068 | 2.47 | 8.79 | 8.13 | 22.64 |
| | | h -Edit-D | 0.243 | 0.071 | 2.38 | 8.62 | 8.16 | 22.85 |
| | Random | EF | 0.241 | 0.059 | 2.75 | 8.57 | 8.15 | 22.49 |
| | | h -Edit-R | 0.242 | 0.065 | 2.46 | 8.42 | 8.18 | 22.68 |
| PnP | Deter. | NP | 0.250 | 0.152 | 1.84 | 8.55 | 8.19 | 25.05 |
| | | NT | 0.251 | 0.144 | 1.58 | 7.94 | 8.24 | 25.53 |
| | | NMG | 0.253 | 0.101 | 2.08 | 9.96 | 8.02 | 23.20 |
| | | PnP Inv | 0.253 | 0.109 | 1.75 | 9.29 | 8.15 | 24.18 |
| | Random | h -Edit-D | 0.254 | 0.158 | 1.51 | 7.28 | 8.33 | 25.68 |
| | | EF | 0.253 | 0.118 | 1.48 | 6.87 | 8.32 | 24.77 |
| | | h -Edit-R | 0.255 | 0.147 | 1.39 | 5.97 | 8.43 | 25.75 |

Table 3. Text-guided editing results with MasaCtrl [6] and Plug-n-Play [70] on PIE-Bench. h -Edit significantly outperforms other baselines in all metrics.



Figure 10. Visualizations of edited images with ρ^{sty} values ranging from $\{1.4, 1.5, 1.6, 1.7, 1.8\}$ for EF + P2P and $\{0.4, 0.5, 0.6, 0.7, 0.8\}$ for h -Edit-R + P2P.



Figure 11. Additional qualitative results of h -Edit-R + P2P and EF + P2P for the combined style and text-guided editing task. Style loss values (lower is better) are displayed below each output image.

F. Ablation Studies

F.1. Impact of \hat{w}^{orig}

| \hat{w}^{orig} | CLIP Sim. \uparrow | Local CLIP \uparrow | DINO Dist. $\times 10^2\downarrow$ | LPIPS $\times 10^2\downarrow$ | SSIM $\times 10\uparrow$ | PNSR \uparrow |
|-------------------------|----------------------|-----------------------|------------------------------------|-------------------------------|--------------------------|-----------------|
| 1.0 | 0.256 | 0.118 | 1.64 | 6.00 | 8.38 | 25.75 |
| 3.0 | 0.255 | 0.137 | 1.52 | 5.49 | 8.44 | 26.36 |
| 5.0 | 0.256 | 0.159 | 1.45 | 5.08 | 8.50 | 26.97 |
| 7.0 | 0.254 | 0.173 | 1.60 | 5.22 | 8.51 | 26.94 |
| 9.0 | 0.241 | 0.172 | 2.30 | 6.44 | 8.40 | 26.03 |

Table 4. Quantitative results of h -Edit-R + P2P when varying \hat{w}^{orig} from 1.0 to 9.0 while keeping w^{edit} and w^{orig} fixed at 7.5 and 1.0, respectively. The best value for each metric is highlighted in bold.

In this section, we study the impact of \hat{w}^{orig} in Eq. 24 by varying its value within $\{1.0, 3.0, 5.0, 7.0, 9.0\}$ while keeping $w^{\text{orig}} = 1$ and $w^{\text{edit}} = 7.5$ fixed for h -Edit-R + P2P. Quantitative and qualitative results are shown in Table 4 and Fig. 12, respectively. The results indicate that increasing \hat{w}^{orig} to a suitable value enhances both editing accuracy and fidelity. For example, raising \hat{w}^{orig} from 1.0 to 7.0 restores the woman’s armor suit in the first row on the left of Fig. 12 while also straightening her hair. Similarly, it effectively removes the balloons in the background while preserving the original appearance of the girl in a red dress in the twelfth row on the left. As discussed in Section A.3, \hat{w}^{orig} controls how much of the original image’s information is excluded during editing. Larger values of \hat{w}^{orig} helps isolate essential information, enabling precise localization of edits. However, excessively high values (i.e., exceeding w^{edit}) may degrade reconstruction quality by removing too much original

information. This is evident in the case of changing colorful paint to drab paint in the last row on the right. These observations suggest that the optimal value of \hat{w}^{orig} is case-dependent, for $w^{\text{edit}} = 7.5$, we found $\hat{w}^{\text{orig}} = 5.0$ achieves the best balance between editing effectiveness and faithfulness.

F.2. Impact of w^{edit}

We investigate the influence of w^{edit} in Eq. 24 for h -Edit-R + P2P by analyzing edited images across different $(w^{\text{edit}}, \hat{w}^{\text{orig}})$ pairs: $\{(7.5, 3.0), (7.5, 5.0), (10.0, 7.0), (10.0, 9.0), (12.5, 9.0), (12.5, 11.0)\}$. Qualitative results are provided in Fig. 13. In general, higher w^{edit} values enhance editing effectiveness, allowing to handle difficult edits. For example, increasing w^{edit} from 7.5 to 12.5 successfully introduces dragons to the images in the final row of Fig. 13. However, higher w^{edit} can degrade reconstruction quality in non-edited regions, requiring a proportional increase in \hat{w}^{orig} to mitigate this effect. Even so, this approach may not succeed in all scenarios. We can overcome this issue by using multiple optimization steps (available for implicit h -Edit). This technique progressively refines edits via applying the score function iteratively, effectively handling challenging cases while maintaining good reconstruction.

F.3. Impact of multiple optimization steps in implicit h -Edit

Fig. 14 highlights the advantage of the implicit version of h -Edit when utilizing multiple optimization steps. Increasing the number of optimization steps significantly enhances editing accuracy while maintaining minimal degradation in reconstruction quality. This capability is unique to the implicit version and cannot be replicated by simply increasing the number of sampling steps. For instance, the explicit version, even with 200 sampling steps, performs only comparably or slightly better than the default implicit version with 50 sampling steps and one optimization step, yet it falls notably short compared to the implicit version with three optimization steps.

Additionally, the effectiveness of multiple optimization steps is evident in the face swapping task, where h -Edit-R with three optimization steps outperforms its one-step counterpart, as presented in Section E.2.

F.4. Comparison between explicit and implicit versions

| Attn. | Steps | Method | CLIP Sim. | Local CLIP \uparrow | DINO Dist. $\times 10^2\downarrow$ | LPIPS $\times 10^2\downarrow$ | SSIM $\times 10\uparrow$ | PSNR \uparrow |
|-------|-------|------------------|-----------|-----------------------|------------------------------------|-------------------------------|--------------------------|-----------------|
| None | 25 | h -Edit-R (ex) | 0.252 | 0.139 | 1.10 | 5.10 | 8.49 | 26.79 |
| | | h -Edit-R (im) | 0.255 | 0.148 | 1.39 | 5.98 | 8.41 | 25.77 |
| | 50 | h -Edit-R (ex) | 0.253 | 0.141 | 1.10 | 5.07 | 8.51 | 27.00 |
| | | h -Edit-R (im) | 0.255 | 0.148 | 1.28 | 5.55 | 8.46 | 26.43 |
| P2P | 25 | h -Edit-R (ex) | 0.254 | 0.153 | 1.38 | 5.04 | 8.50 | 26.81 |
| | | h -Edit-R (im) | 0.255 | 0.150 | 1.38 | 5.03 | 8.50 | 26.88 |
| | 50 | h -Edit-R (ex) | 0.256 | 0.158 | 1.47 | 5.10 | 8.50 | 26.85 |
| | | h -Edit-R (im) | 0.256 | 0.159 | 1.45 | 5.08 | 8.50 | 26.97 |

Table 5. Quantitative comparison of h -Edit-R implicit and explicit forms, with and without P2P, evaluated over 25 and 50 sampling steps.

In this section, we compare the explicit and implicit versions of h -Edit-R with and without P2P, using either 25 or 50 sampling steps. Without P2P, the implicit version generally performs more accurate edits than the explicit counterpart, though the results vary by case, as shown in Table 5 and Fig. 15. However, when combined with P2P, the two versions perform comparably. Instances where implicit h -Edit-R outperforms the explicit version, and vice versa, are illustrated in Fig. 16. Our preference for the implicit version as the default is not primarily due to its performance relative to the explicit version but rather its ability to support multiple optimization steps, which offers greater flexibility.

F.5. Face swapping without masks

We demonstrate that our h -Edit-R method can perform face swapping without relying on mask postprocessing techniques for reconstruction, with qualitative results of h -Edit-R (3s) shown in Fig. 17. h -Edit-R without masks achieves near-perfect faithful reconstruction, with minor background changes. For instance, in the third row (left), it preserves background text, while in more complex backgrounds, such as dense text (last row, right) or intricate shirt patterns (last row, left), it maintains individual features with slight background blurring. This capability is unique to our method, as state-of-the-art approaches like DiffFace and FaceShifter rely on masks for faithful reconstruction. These findings suggest that in scenarios where masks are unavailable, our method is a robust choice for face editing with minimal reconstruction error.

| Inv. | Attn. | Method | Time (s)↓ |
|--------|-------|------------------|--------------|
| Deter. | P2P | NP | 21.68 |
| | | NT | 186.84 |
| | | StyleD | 467.16 |
| | | NMG | 35.67 |
| | | PnP Inv | 37.65 |
| | | <i>h</i> -Edit-D | 48.63 |
| Random | None | EF | 23.20 |
| | | LEDITS++ | 18.31 |
| | P2P | <i>h</i> -Edit-R | 33.07 |
| | | EF | 32.95 |
| | | <i>h</i> -Edit-R | 50.21 |

(a) Editing time for text-guided editing methods

| Method | Time (s)↓ |
|-----------------------|-------------|
| FaceShifter | 1.31 |
| MegaFS | 2.29 |
| AFS | 1.03 |
| DiffFace | 46.42 |
| EF | 26.11 |
| <i>h</i> -edit-R | 26.34 |
| <i>h</i> -edit-R (3s) | 51.36 |

(b) Editing time for face swapping methods

| Inv. | Attn. | Method | Time (s)↓ |
|--------|-------|------------------|--------------|
| Random | P2P | EF | 44.32 |
| | | <i>h</i> -Edit-R | 50.68 |

(c) Editing time for combined text-guided and style editing methods

Table 6. Editing times per image (in seconds) of our method and baselines across three tasks: text-guided editing (left), face swapping (top right), and combined text-guided and style-based editing (bottom right). Experiments were conducted on an NVIDIA V100 GPU 32GB.

F.6. Running time

Table 6 shows the editing times per image of our method and baselines for three editing tasks: text-guided editing, face swapping, and combined text-guided and style editing.

In the text-guided setting, among deterministic-inversion-based methods, *h*-Edit-D + P2P requires longer computation time (48.63s) than NP + P2P (21.68s), PnP Inv + P2P (37.65s), and NMG + P2P (35.67s) due to additional U-Net calls for reconstruction and editing term computation. However, this additional 12-second overhead compared to PnP Inv + P2P yields significantly improved performance, with a 0.05 increase in local CLIP Similarity and 0.6×10^{-2} better LPIPS (Table 1). While NP + P2P achieves the fastest processing time by simply substituting source embedding for null embedding during editing, it suffers from substantially lower reconstruction quality. Our favorable trade-off between computation time and editing quality extends to comparisons with random-inversion-based methods. LEDITS++ is the fastest as they leverage high-order solvers [13, 43, 84] - a feature that could also be incorporated into our method.

In the face swapping task, diffusion-based methods generally require longer processing time per image compared to GAN-based methods (FaceShifter [37]: 1.31s) or StyleGAN-based approaches (MegaFS [86]: 2.29s, AFS [71]: 1.03s) due to their iterative sampling nature. Among diffusion-based methods, *h*-Edit-R (26.34s) and EF (26.11s) achieve the fastest processing times. Despite sharing the same sampling steps, *h*-Edit-R outperforms DiffFace (46.42s) in efficiency as DiffFace requires additional gaze detection and face parsing models at each step, beyond the common ArcFace computation. While our *h*-Edit-R with 3 optimization steps variant shows slightly increased computation time (51.36s), it achieves better ArcFace ID similarity compared to DiffFace with comparable reconstruction quality. Notably, as training-free approaches, our method and EF offer immediate deployment advantages over DiffFace and GAN-based methods that require task-specific training.

In the combined text-guided and style editing task, *h*-Edit-R + P2P (50.68s) shows only a moderate increase from its text-guided variant (50.21s) by avoiding U-Net backpropagation for style editing. In contrast, EF + P2P with FreeDom [79]’s technique requires additional backpropagation computation, resulting in a larger time increase from its text-guided counterpart (32.95s to 44.32s).

G. Analysis on Metrics

During our text-guided editing experiments, we observed that CLIP similarity and DINO distance metrics could yield inconsistencies between quantitative and qualitative results. For CLIP similarity, we hypothesize that this occurs because the attribute being edited often constitutes only a small portion of the target prompt. In such cases, even accurate edits may result in minor improvements in CLIP similarity, whereas unintended changes to other attributes can lead to significant drops. Consequently, methods that make no edits and simply preserve the original image may achieve comparable or better CLIP similarity scores than methods that successfully perform challenging edits. This phenomenon is evident with NP and NT - the two strong editing methods capable of handling challenging edits more effectively than PnP Inv, as shown in Fig. 5.

However, their CLIP similarity scores are lower than that of PnP Inv, as illustrated in Table 1.

In the case of DINO distance, since this metric is computed on the entire image rather than the non-editing region, it can yield poor results in significant editing scenarios like changing background color or removing objects even when original non-editing content is perfectly preserved.

H. Ethical Considerations

Our work aims to advance the development of effective and efficient diffusion-based image editing methods, fostering contributions to both academic research and real-world applications. However, we recognize that these advancements could be misused for harmful purposes, such as generating misinformation or damaging individuals' reputations. To address these risks, it is crucial to implement safeguards that detect and prevent unethical applications. One potential approach is to employ a detection framework that analyzes edited images and flags or discards outputs that violate ethical guidelines or pose potential harm to society. Such proactive measures can help ensure that this technology is used responsibly and ethically.



Figure 12. Qualitative results of h -Edit-R + P2P when varying \hat{w}^{orig} from 1.0 to 9.0 while keeping w^{edit} and w^{orig} fixed at 7.5 and 1.0, respectively. Increasing \hat{w}^{orig} to an appropriate value improves both editing accuracy and fidelity.

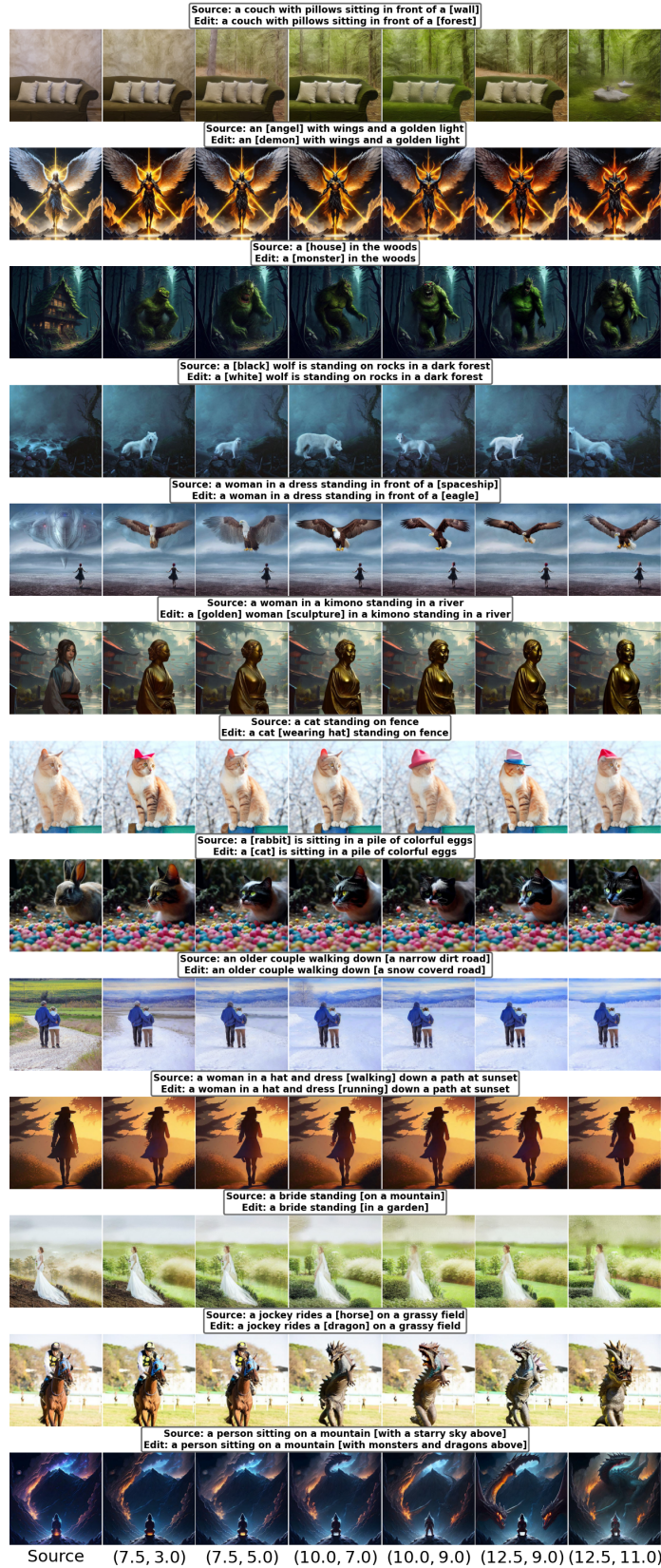


Figure 13. Qualitative results of h -Edit-R + P2P when varying $(w^{\text{edit}}, \hat{w}^{\text{orig}})$ within $\{(7.5, 3.0), (7.5, 5.0), (10.0, 7.0), (10.0, 9.0), (12.5, 9.0), (12.5, 11.0)\}$. Higher w^{edit} values effectively handle challenging edits but may compromise reconstruction quality.

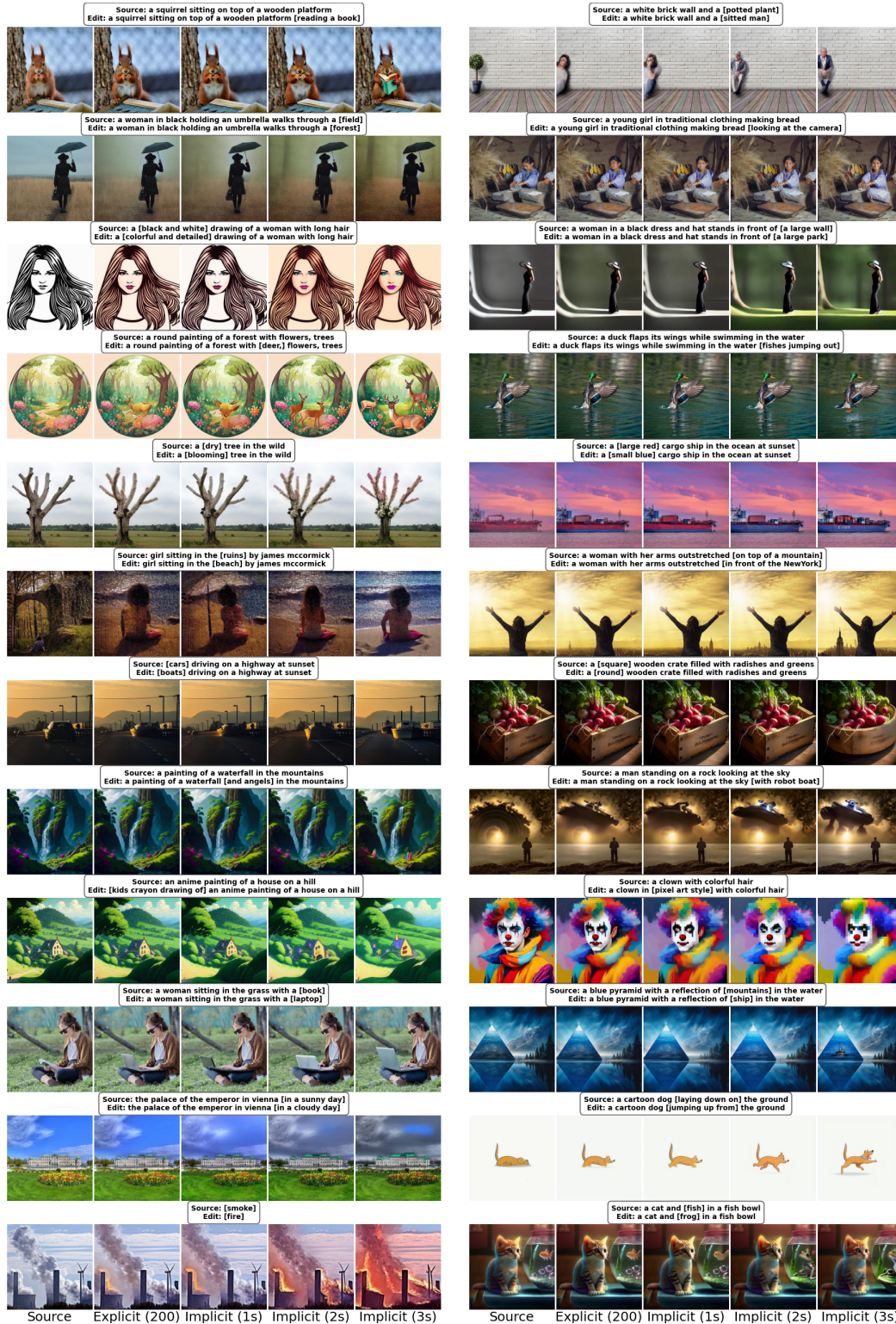


Figure 14. Qualitative examples of implicit h -Edit-R + P2P with 50 sampling steps using one, two and three optimization steps (1s/2s/3s), compared to its explicit counterpart with 200 sampling steps. More optimization steps effectively handle challenging cases, outperforming increased sampling steps in the explicit form.

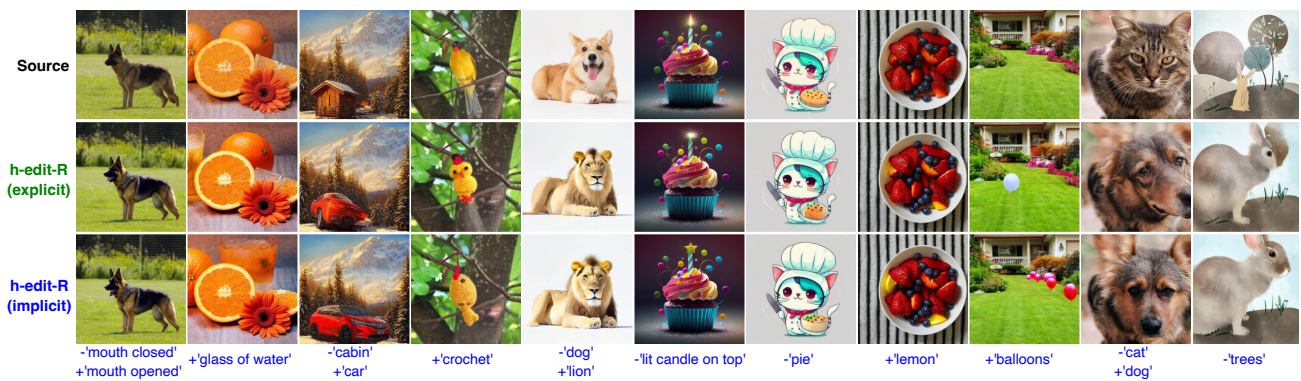


Figure 15. Qualitative visualizations comparing the explicit and implicit versions of h -Edit-R with 25 sampling steps.



Figure 16. Qualitative visualizations comparing the explicit and implicit versions of h -Edit-R + P2P with 25 sampling steps.



Figure 17. Swapped faces generated by h -Edit-R (3s) with and without masks.